PLASMODIUM EXOERYTHROCYTIC PARASITES REDIRECT TRAFFICKING OF HUMAN PROTEINS TO THE PARASITOPHOROUS VACUOLE

Jaeson Calla[1], Nimisha Mittal[1], Greg LaMonte[1], Benjamin Liffner[2], Karla P. Godinez-Macias[1], Krypton Carolino[1], Gregory T. Walker[1], Bing Yu Zou[1], Emma Paytas[1], Layné Guerra[3], Carlos Tong-Rios[3], Brice Campo[4], Joseph M. Vinetz[3,5], Dionicia Gamboa[3], Manuela Raffatellu[1,6,7], Sabrina Absalon[2], and Elizabeth A. Winzeler[1]

Affiliations:

[1]Department of Pediatrics, Division of Host-Microbe Systems & Therapeutics, School of Medicine, University of California, San Diego, La Jolla, United States of America.

[2]Department of Pharmacology and Toxicology, Indiana University School of Medicine, Indianapolis, United States of America.

[3]Laboratorio ICEMR-Amazonia, Laboratorios de Investigación y Desarrollo, Facultad de Ciencias y Filosofía, Universidad Peruana Cayetano Heredia, Lima, Peru.

[4]Medicines for Malaria Venture, Geneva, Switzerland.

[5]Current address: Department of Internal Medicine, Section of Infectious Diseases, School of Medicine, Yale University, New Haven, United States of America.

[6]Center for Microbiome Innovation, University of California San Diego, La Jolla, United States of America.

[7]Chiba University-UC San Diego Center for Mucosal Immunology, Allergy, and Vaccines (CU-UCSD cMAV), La Jolla, United States of America.

To whom correspondence should be addressed: ewinzeler@health.ucsd.edu (EW)

KEYWORDS

Hypnozoite, malaria, *P. vivax*, Hepatocyte.

ABBREVIATIONS USED

PVR, Parasitophorous Vacuole Region; NR4A3, Nuclear receptor subfamily 4 group A member 3, HCI, High Content Imaging; qRT-PCR quantitative Reverse Transcriptase Polymerase Chain Reaction; ATQ, Atovaquone; EEF, Exoerythrocytic form; FC, flow cytometry; FACS, Fluorescence-Activated Cell Sorting; hpi, hours post infection; TRAP, Thrombospondin Related Anonymous Protein; GOLGA8A, Golgin subfamily A member 8A; MUC13, Mucin 13; CGA, Glycoprotein hormones alpha chain; Binding immunoglobulin protein, BiP; CXCL2, Chemokine

(C-X-C Motif) Ligand 2; CSP, Circumsporozoite protein; UIS4, Up-regulated in infective sporozoites gene 4; Lipopolysaccharide, LPS.

ABSTRACT

Changes in host cell morphology and transcription after apicomplexan parasite infection have long been noted, but there have been few studies of the functional consequences of host cell remodeling. Here we show, using time-dependent immunofluorescence microscopy of multiple human cell lines (HepG2, HC-04, Huh7.5.1 and primary human hepatocytes), infected with multiple *Plasmodium* species (*Plasmodium berghei, P. falciparum* and *P. vivax* (hypnozoites and schizonts)), and antibodies to multiple human proteins (HsNR4A3, HsMUC13, HsGOLGA8A, HsCGA, HsBiP, HsCXCL2), that human protein trafficking is extensively modified in *Plasmodium* infected cells. Using conventional as well as ultrastructure expansion microscopy we show that newly-synthesized human proteins are trafficked to the parasitophorous vacuole instead of the infected-cell plasma membrane, nucleus or extracellular space. Universal redirection of human signaling proteins cells the parasitophorous vacuole may provide a mechanistic explanation for how apicomplexan parasites can block host cells response to infection.

INTRODUCTION

Malaria remains a worldwide problem with up to 241 million cases reported in 2021[1]. Given the economic and humanitarian burden of malaria, and the continual emergence of parasite resistance to drugs that act against the symptomatic stages of the infection, new strategies to treat, prevent or control malaria are needed.

Liver cells are the primary cellular target of the *Plasmodium* parasite's exoerythrocytic stage. After injection into the vertebrate host by the bite of an infected Anopheline mosquito, the parasites (sporozoites) travel to the liver where they migrate and cross through several barriers. These barriers include endothelial cells, dermal fibroblast, liver sinusoidal endothelial cells (LSECs) and highly phagocytic Kupffer cells, that allows sporozoites to pass all barriers to find and infect hepatocytes[2,3]. When a suitable hepatocyte is reached, they inject the contents of their apical organelles using their specialized secretory organelles, the micronemes and rhoptries, into the hepatocyte membrane creating a molecular machine that enables the formation of a vacuole in the host cell cytoplasm[4]. The vacuole will enclose and protect the parasite and is surrounded by a host-derived parasitophorous vacuole membrane (PVM)[5]. Similar vacuoles are formed when

blood stage malaria parasites invade erythrocytes and by other apicomplexan parasites, including *Toxoplasma gondii* when they invade fibroblasts, for example[6]. Some malaria parasite species can also remain in the liver in a dormant state, called a hypnozoite[7]. Hypnozoite-forming species, especially *P. vivax*, represent barriers to malaria eradication because if they are not eliminated by drug treatment, they can reawake months to years later, leading to patient relapse, as well as active malaria transmission in an area that was once cleared of malaria. Despite their importance, hypnozoites are poorly understood.

There are no clinical symptoms associated with liver stage infection[8]. Fever and chills that are characteristic of malaria only develop after the merozoites are released from the schizont and move to the circulatory system scanning for their next target cells, the erythrocytes.

Pre-erythrocytic stages are the primary target for the development of malaria vaccines. It has been suggested that vaccines directed at this stage will be more effective because they will suppress the spread of vaccine-resistance because of low parasite numbers at this stage (hundreds versus billions in blood stages) and the only licensed vaccine, RTS, S/AS01, Mosquirix™, consists of a target, circumsporozoite protein (CSP), which is highly expressed in *Plasmodium* sporozoites[9-11]. Irradiated sporozoites also provide strong protection against malaria and have been used in vaccine trials[12-14]. Irradiated sporozoites invade hepatocytes, form a trophozoite, but then the host cell will apoptose before merozoite maturation is complete, allowing the display of antigens and potentially elicit an improved immune response that is missing with unirradiated sporozoites[15]. Vaccination with parasites that have mutations in PV-localized UIS3 and UIS4 result in an unprotective infection and sterile protection against challenge[16].

In the course of their development, erythrocytes will have shed many of their organelles, including their nuclei, before they become susceptible to invasion by malaria parasites. Hepatocytes, on the other hand, have nuclei and remain transcriptionally active after parasite invasion. We had previously performed a dual RNAseq study on flow-sorted, *P. berghei*-infected liver cells[17]. The experiments, which were conducted in a variety of time points and on different cell types showed concerted patterns of gene upregulation, including genes involved in the immune response, such as the mucin, *HsMUC13*[17]. Curiously, we observed that HsMUC13 protein colocalized with parasite UIS4, a protein inserted into the PVM in infected cells[17]. To further

investigate these phenomena, here we examine other human genes that were upregulated after parasite infection, including the orphan human nuclear hormone receptor, *HsNR4A3*.

Surprisingly, we find that the cognate protein for all upregulated human genes that we examine show colocalization with the parasite parasitophorous vacuole (PV) marker, UIS4[18]. We show this colocalization is observed not only for *P. berghei* and *P. falciparum* liver stages, but for both *P. vivax* schizonts and hypnozoites as well. Furthermore, using ultrastructure expansion microscopy, a recently developed sample preparation method that enabled the isotropic expansion of *Plasmodium* parasites up to 4.5-fold[19], we revealed the association of HsNR4A3 proteins with the PVM of *P. berghei* parasite. Our data indicate that in all these parasites, host proteins are being redirected to the PV. We propose that apicomplexan parasites manipulate host secretion apparatus to favor their development and to hide from the immune system.

RESULTS

Host proteins are transcriptionally upregulated during P. berghei infection of liver cells

A previous dual (parasite and human) RNA-seq study with the rodent malaria parasite, *P. berghei* (*Pb*GFP-SM$_{CON}$ (*Pb*-GFP)), identified a series of human transcripts that were upregulated during parasite exoerythrocytic infection (Fig. 1a, 1b). Multiple time points, replicates, and different hepatoma host cells (HepG2s, Huh7.5.1s, HC-04s) were used in these experiments in which human cells were individually sorted into infected and noninfected pools based on the presence of parasite-encoded GFP signal. Oddly, the most upregulated and statistically significant genes across cell lines at 48 hours did not seem to be functionally related to one another. *HsMUC13* encodes a secreted membrane localized mucin that is usually expressed in the gut. It is normally upregulated after infection and is asymmetrically localized to luminal side of gut epithelial cells[20]. We had previously shown that it colocalized to the parasite vacuole in mature *P. vivax* and *P. berghei* schizonts[17]. Also upregulated in multiple hepatocyte-derived lines was *HsNR4A3* ($p = 2.8x10^{-30}$). The NR4A subfamily encodes orphan nuclear receptors that belong to the larger nuclear receptors (NRs) superfamily of eukaryotic transcription factors. The NR4A subfamily includes three members, namely NUR77 (HsNR4A1), NURR1 (HsNR4A2) and NOR1 (HsNR4A3), which are gene regulators and participate in diverse biological functions. Although exact function of

HsNR4A3 is not known, data suggest a potential role in controlling glucose in some cell types[21]. NR4A3 knockout mice show expansion of the pancreatic beta cells, needed for insulin production, and NR4A3 overexpression lines increase glucose production in response to some stimuli, and act as activator of beta cell proliferation and insulin production[22,23]. It has also been reported as an NLRP3 inflammasome activation-responsive gene[24]. In the cancer arena, it has been shown that NR4A3 overexpression attenuates proliferation of cancer cells and promotes apoptosis by augmenting the expression of pro-apoptotic genes via a p53 dependent mechanism[25]. *HsCGA* (adjusted $p = 4.4\text{x}10^{-13}$) encodes the shared alpha chain of the heterodimeric human glycoprotein hormones; thyrotropin/thyroid stimulating hormone/TSH, lutropin/luteinizing hormone/LH, follitropin/follicle stimulating hormone/FSH and choriogonadotropin/CG. HsCGA, along with its partner, would normally be secreted into the bloodstream where it would bind rhodopsin-like G protein-coupled receptors on the target cell[26]. *HsCGA* is expressed at high levels in the placenta but is also upregulated in breast cancer and is an estrogen receptor alpha (ERα)-responsive gene in human breast tumors[27]. *HsTAS2R4* encodes a G-protein coupled receptor that is normally expressed on the surface of tongue epithelial cells. It is responsive to bitter molecules, including, interestingly, the antimalarial, quinine but may also play a role in small molecule-sensing in extraoral cell types[28].

In addition, the set of statistically significant upregulated genes included several noncoding genes. The lncRNA, *HsNEAT1* (adjusted $p = 1.8\text{x}10^{-34}$), promotes activation of inflammasomes in macrophages[29]. *HsMALAT1*, also known as *HsNEAT2* is also a large, non-coding RNA, which is highly conserved amongst mammals and highly expressed. Overexpression of *HsMALAT1* suppresses breast cancer metastasis in transgenic, xenograft, and syngeneic models of cancer[30] and is also strongly associated with inflammasome activation[31].

Because the RNAseq studies had been performed on model hepatoma cells lines we used qRT-PCR to confirm the upregulation of *HsNR4A3, HsMUC13, HsCGA, HsSLC22A8, HsMALAT1, HsRASSSF9, HsSDHA, HsSLC25A27, HsNEAT1,* and *HsTAS2R4* in *P. berghei*-infected primary human hepatocytes, as well as in *P. berghei* infected Huh7.5.1, HepG2 and HC-04 cells. Cells were infected with *P. berghei* expressing GFP and flow sorted. RNA was extracted from infected cells, as well as from control, parallel non-infected cells. In these four cell lines, we observed consistent 13-20-fold upregulation of *HsNR4A3* in all cell lines except for HepG2 cells

(Fig. 1c). We also observed upregulation of other transcripts via qRT-PCRs but not as consistently across all lines.

To further ensure that the patterns were not specific to parasites, we performed Western blot analysis. We obtained several commercial antibodies to some of the different human proteins that showed the highest, most significant, and reproducible upregulation. These included HsNR4A3, HsCGA, and HsMUC13. HsGOLGA8A, was also included (probability of upregulation of chance = 4.04×10^{-10}). It encodes a member of the Golgin family of membrane proteins which play a role in tethering vesicles to the Golgi apparatus[32],[33]. All 21 annotated Golgins were amongst the set of upregulated genes in infected cells, 13 significantly (hypergeometric mean probability of enrichment by chance = 5.5×10^{-5}), with an average upregulation of 2.3×. The bulk cultures as well as uninfected HC04 control cultures were infected with both *P. berghei* and *P. falciparum*. All the evaluated antibodies showed recognition of a single band corresponding to the native protein (Fig. S1a, S1b). In some cases, upregulation was observed relative to human control protein (Hs-Vinculin, Fig. S1b), but given that only a small proportion of cells are infected in bulk cultures (1 to 2%), especially with *P. falciparum*, we did not attempt to further quantify this. The antibody to CGA1 recognized a larger than expected protein. CGA1 is heavily glycosylated which may contribute to the size difference.

Upregulated host proteins show colocalization with PVM via immunofluorescence analysis.

Given the challenges of analyzing level by Western we next used immunofluorescence and confocal microscopy to confirm our RNA-seq results. First, assays were performed with mature *P. berghei*, the species on which hepatocyte flow sorting was performed. Isolated *P. berghei* sporozoites were incubated with a permissive human liver cell line, HC-04. After 48 hours, the cultures were fixed and stained with a set of primary commercial antibodies against various upregulated hepatocyte proteins (HsNR4A3, HsCGA, HsGOLGA8A, and HsMUC13), and to parasite UIS4 (Fig. 2a), a parasite protein highly expressed in sporozoites and liver stages of multiple *Plasmodium* species, and which localizes to the PVM in both hypnozoites and schizonts[34]. All antibodies (against HsNR4A3, HsCGA, HsGOLGA8A, and HsMUC13 proteins) showed high expression of their cognate proteins in *P. berghei*-infected but not -uninfected HC-04 cells. Interestingly, all four host proteins colocalized with the parasite marker, UIS4 (Fig. 2a). HsNR4A3

is normally localized to the nucleus[35] and indeed staining was observed in the nucleus in uninfected cells visible in the image. A zoom in (Fig. 2a1), a panoramic view (Fig. 2a2), and a panoramic overexposed view (Fig. 2a3) is also shown for the HsNR4A3 protein. GOLGA8A encodes protein with an N-terminal coiled-coil domain and a single C-terminal transmembrane domain and is also known as golgin-67. It localized to the Golgi apparatus which in most human cells is adjacent to the nucleus[36]. As expected, our staining showed weak HsGOLGA8A surrounding the nucleus in uninfected cells. MUC13 and CGA are both expected to be secreted into the extracellular space. Uninfected cells showed some weak diffuse cytoplasmic staining with antibodies to these proteins.

To determine if similar staining would be observed in human cells infected with the human pathogen, *P. falciparum,* we performed experiments using dissected *P. falciparum* sporozoites and primary hepatocytes. Sporozoites were placed on primary hepatocytes in 96-well plates and cultures were incubated for 120 hours, necessary because of the longer *P. falciparum* liver development time. Immunofluorescence was performed using a *P. vivax* antibody to PvUIS4[34] (which is cross-reactive with PbUIS4, and PfUIS4) (Fig. 2b) and anti-human primary antibodies. These experiments confirmed upregulation of the HsNR4A3, HsCGA, HsGOLGA8A, and HsMUC13 proteins with staining, as with *P. berghei*, occurring in the PVM region, overlapping largely with UIS4 staining. Importantly, these data showed that the staining patterns were not associated with the use of a hepatoma cell line and were conserved in primary human hepatocytes.

We next examined another human pathogen, *P. vivax,* which can remain in an infected liver cell as a hypnozoite that can be activated months or years after the primary infection. As *P. vivax* cannot be maintained in cell culture, patients diagnosed with *P. vivax* malaria, were recruited, and asked to provide 20mL of whole blood, which was used to feed fasted, female *Anopheles darlingi* mosquitoes using a standard membrane feeding assay. After 14 days the mosquitoes were dissected to obtain sporozoites, which were used to infect HC-04 cell lines (see Methods). After five days, the cells were fixed and stained with our primary antibodies (against HsNR4A3, HsCGA, HsGOLGA8A, and HsMUC13 proteins). Again, all antibodies showed strong colocalization with the parasites (Fig. 2c) for all proteins.

To determine whether this pattern would be observed for hypnozoites we searched for UIS4 positive objects that were smaller than 10µm and which showed characteristic circular patterns

associated with UIS4 signal, the bonafide way to identify hypnozoites[34]. For our *P. vivax* infected samples, we identified hypnozoites at a rate of 1 per 5,000 hepatocytes, and schizonts at a frequency of ~1:1,000, some of which are shown in Fig. 2d. Interestingly, the same immunofluorescent micrographs also showed colocalization with HsNR4A3, HsCGA, HsGOLGA8A, and the HsMUC13 (Fig. 2d), a zoom-in for HsNR4A3 protein in hypnozoites stages is shown (Fig. 2d1). In fact, previous parasite-associated immunolocalization had been observed for HsMUC13[17]. Analysis of the images showed a strong correlation between UIS4 and the different tested proteins for all species (Fig. S2).

While the relocalization of one protein could be functional, the relocalization of all was puzzling. These micrographs showed similar localization of the human proteins, ruling out the possibility of the species-specific secondary antibodies cross-reacting with the primary UIS4 antibody. In addition, we repeated IFAs with a variety of different primary antibodies using the *P. berghei* infection model and in all cases, the same patterns were obtained (Fig. S3).

HsNR4A3 edited lines show decreased NR4A3 staining in Westerns and IFA

To further assess the question of antibody specificity as well as HsNR4A3 functionality, we next performed knockouts on *HsNR4A3*. We used CRISPR/*Cas9*-based methods to disrupt *HsNR4A3* in clonal HC-04 cell lines using two different approaches (two plasmid or single plasmid) and different guide RNA sets (Fig. S4a and S4b), obtaining six different stably edited clones (GL1, GL2, and GL3 and NM1, NM2, and NM3 created using the two approaches)). Western blot analysis showed lower expression of HsNR4A3 in five of six clones (clones GL1 and GL3 and NM1, NM2, and NM3)) relative to native HC-04 cells (Fig. S4c, S4d).

To evaluate antibody specificity, *HsNR4A3* knockout cells were infected with *P. berghei* (*Pb*-ANKA-GFP-Luc SMCON (*Pb*-Luc)) sporozoites. After 48hpi, the infected and uninfected cells were evaluated by immunofluorescence and confocal microscopy. For HC-04 HsNR4A3 unmodified cells (WT) we observed colocalization with the parasite markers UIS4 (Fig. S4e) and HSP70 (Fig. S4e, S4f). In contrast, no NR4A3 staining was observed in *HsNR4A3* knockout cells (Fig. S4e) and pattern quantification showed no correlation ($p < 0.0005$) Fig. S4f). Staining was similar to the negative control in which the NR4A3 antibody was not used. These data largely rule

out the possibility of NR4A3 antibody cross-hybridization with an as-yet unspecified parasite protein.

To confirm our findings in *P. vivax*, we also performed *in vitro* infection tests using cloned GL1 and GL3 *HsNR4A3* knockout cells and *P. vivax* parasites obtained as described above. We observed a marked expression of the HsNR4A3 protein in the HC-04 HsNR4A3 WT cells in the two stages of the parasite (hypnozoites and schizonts) showing the expected co-staining with UIS4. For clone GL1, we did not identify any parasites (see below) while for clone GL3 (Fig. S4g), we observed no signal or co-staining with UIS4. A statistically-significant loss of staining correlation in *HsNR4A3* knockouts was confirmed by image quantitation (Fig. S4h, S4i).

Role of the protein HsNR4A3 in exoerythrocytic infections

To determine whether HsNR4A3 contributes to parasite growth and development we investigated both schizont size, schizont number and schizont morphology in the *HsNR4A3* knockout clones in *P. berghei* and *P. vivax*. First, *in vitro* infections with *P. berghei* parasites were carried out. We performed a qRT-PCR experiment using primers to the *P. berghei* 18S RNA gene as previously described[37]. These data showed that a higher number of cycles were needed to detect parasites in NM1, NM2 and NM3 clones, with NM3 requiring almost as many cycles for detection as treatment with 5 nM atovaquone, a drug which completely blocks parasite exoerythrocytic development (Fig. S5a). Next, high content imaging analysis was performed on *P. berghei* infected cells and used to determine the number of UIS4 positive objects per field ($0.8cm^2$). These data showed a ~70% reduction in the relative number of parasites in all three *HsNR4A3* knockout clones (Fig. S5b). We also observe that most of the positive objects identified in *HsNR4A3* knockout cells (NM1-NM3) have a diameter of 5 µm compared with 40µm the WT HC-04 cells (Fig. S5c).

To investigate the role of HsNR4A3 in *P. vivax* development, we infected our GL1 and GL3 *HsNR4A3* knockout lines with *P vivax* sporozoites, obtained as described above, and allowed the parasites to develop for 120 hours. Cultures were co-stained with the UIS4 parasite marker to identify and count infected cells. Hypnozoites were distinguished from schizonts based on parasite size (Fig. S5d, S5e). In both clones we observed fewer schizonts, although the reduction in the number of hypnozoites was not as marked. This suggests that the expression of the HsNR4A3 protein is needed for the *P. vivax* parasite to complete the schizont maturation process. To

determine if this was true for *P. berghei* as well, we also infected the *HsNR4A3* knockout clones with GFP-expressing *P. berghei* sporozoites and performed flow sorting of GFP-positive objects on GL1 and WT HC-04 cells after 48 hours incubation (Fig. S5f). We observed a marked reduction in the number of GFP positive objects in GL1. These data suggest that HsNR4A3-depleted HC-04 cells may be less able to support parasite invasion and maturation but also highlight that different clones have different levels of gene disruption in diploid human cells, and the phenotype is slightly inconsistent.

On the other hand, all experiments described above were normalized to the number of human cells (at either the cell counting level or via total RNA in the qPCR studies) and if human cells grew faster this would contribute to lower relative parasite numbers after a 48-hour incubation and an even greater reduction with P. vivax infections. Because it has been reported that HsNR4A3-edited human breast and lung cancer cells (MDA-MB-231 and H1299, respectively) show increased cell proliferation[25], we measured growth rates in the NM1 and NM3 clones and indeed observed 3 to 6 × more cells in comparison to the HC-04 HsNR4A3 WT cells 36 hours after plating. Thus, although we do find that HsNR4A3 expression may help the parasites survive and grow, the impact could be partially indirect.

HsNR4A3 is trafficked to the parasitophorous vacuole membrane.

As a nuclear hormone receptor, HsNR4A3 is expected to traffic between the nucleus and cytoplasm. To study the temporal dynamics of HsNR4A3 relocalization in the context of a parasite infection we next conducted a time course experiment in *P. berghei,* monitoring subcellular localization of HsNR4A3 during exoerythrocytic infections. *P. berghei* sporozoites were placed on HC-04 cells and samples were collected and fixed for immunofluorescence analysis every three hours. At three hours, HsNR4A3 staining was observed in the host cell nucleus, overlapping with host cell DAPI for both infected and uninfected cells, as expected for a nuclear hormone orphan receptor, which are constitutively-active transcription factors (Fig. 3). In contrast, the parasite-specific marker, UIS4, was clearly in the host cell cytoplasm, surrounding the parasite and only found in infected cells. At later time points, HsNR4A3 was no longer found in the host nucleus, and was now found in the cytoplasm of infected cells. By 12 hours, weak HsNR4A3 staining was observed in the nucleus of uninfected cells, but strong staining was observed in infected cells in

the PVR. In late stages (24-72 hours), HsNR4A3 expression overlapped with the parasite marker, UIS4 (Fig. 3a, 3b). Given the clear upregulation in NR4A3 gene expression in infected cells, these patterns are consistent with newly synthesized NR4A3 being trafficked directly into the PVR instead of to the host nucleus. Image quantification (Fig. S6a) showed little PbUIS4:HsNR4A3 correlation at early times (<0.1 at 3 hours) but strong correlation at later times (>0.9 at 96 hours), and an inverse relationship with DAPI:HsNR4A3 correlation (Fig. S6b). Similar relocalization patterns were also observed over the course of *P. berghei* exoerythrocytic development for HsGOLGA8A (Fig. S7a, S7b) with the staining observed around the HC-04 cell nucleus at time zero and then moving to co-localize with PbUIS4 by 48 hours in infected cells only. As a control, we examined a gene that did not show differential regulation after infection. HsBiP, also known as HsHSPA5 or GRP-78 is a highly expressed heat shock protein that is typically found in the lumen of the ER and is a well-established marker of ER. It shows little evidence of differential regulation after infection in our dual RNAseq study ($p = 0.97$, log2fold change = -0.006) but is one of the most abundant transcripts (ranking at 96 of ~25,000 transcripts in terms of base mean expression). Although in early stages of development it surrounded the host nuclei (Fig. S7c) as predicted in all eukaryotic cells, it completely colocalized with PbUIS4 by 72 hours of infection and image analysis showed strong correlation with PbUIS4 (Fig. S7d).

Expansion immunofluorescence confocal microscopy localizes hsNR4A3 to the parasitophorous vacuole.

To further characterize the interaction of HsNR4A3 with the PVM we turned into ultrastructure expansion microscopy (U-ExM) coupled with Airyscan super-resolution microscopy[19,38]. We fixed and expanded Huh7.5.1. cells after 48 hours of infection with *P. berghei* parasites. Previous work in blood-stage parasites demonstrated that the higher resolution achieved post-expansion allows to distinguish the PVM from the parasite plasma membrane both stained by Bodipy-TR-ceramide dye[38]. Using anti-UIS4 antibody in combination with Bodipy-TR ceramide staining we expectedly localized UIS4 at the PVM and observed numerous UIS4-positive lipid-enriched vesicles within the PV space or in the host-cytoplasm (Fig. S8). After the validation of UIS4 as U-EXM compatible PVM marker, we used primary antibodies against HsNR4A3 and UIS4 proteins and confirmed the close association of HsNR4A3 with the PVM. HsNR4A3 localized at the host-cytosolic side of the PVM in foci that predominantly are uniformly distributed

326 around the PV and occasionally concentrated in pockets associated with the PVM with some
327 staining in the PV (Fig. 4a).

328

329 *Secreted immune signaling molecules are also redirected to the PVR*

330 One unifying hypothesis that could explain the colocalization that was observed with many
331 of our examined proteins would be if all newly synthesized inter and intracellular host signaling
332 molecules were redirected away from their usual cytoplasmic or cell membrane location and into
333 the parasite vacuole membrane region PVM, potentially as a way to avoid immune signaling or
334 instructions to undergo apoptosis. To further investigate this, we examined the list of upregulated
335 genes to identify well-characterized cytokines and selected HsCXCL2 (Fig S9a, S9b), which was
336 expressed and upregulated in infected HC-04 cells in particular (log_2 fold change = 2.76, p =
337 1.46×10^{-07}). *HsCXCL2* encodes a chemokine ligand that is secreted by monocytes and
338 macrophages at the site of inflammation and is strongly responsive to LPS stimulation. It binds to
339 the chemokine receptor, HsCXCR2 and plays a role in early stage of neutrophil recruitment during
340 tissue inflammation[39]. To test the hypothesis that HsCXCL2 would migrate to the PVR after
341 immune stimulation HC-04 cells were first infected with *P. berghei* and then after 24 hours treated
342 with LPS. Immunofluorescence assays using a CXCL2 antibody were performed at 2, 24 and 48
343 hours (26, 48 and 72hpi). These data showed a strong upregulation of CXCL2 expression in LPS-
344 treated, infected and uninfected HC-04 cells. As with other host proteins, HsCXCL2 staining
345 colocalized with the PVR and PbUIS4 in the infected cells (Fig. 5a, 5b). The specificity of
346 commercial antibodies against HsCXL2, HsBiP (Fig. S10a – Fig. S10d) and the controls (Fig.
347 S10e – Fig. S10f) are showed.

348 **DISCUSSION**

349 Here we have shown that five different upregulated proteins (HsNR4A3, HsCGA,
350 HsGOLGA8A, HsMUC13, and HsCXCL2), each with different, intracellular trafficking patterns,
351 all end up in the PV or PVR, surrounding the parasite. In addition, this pattern has also been
352 observed by others with unrelated proteins: Posfai and coworkers observed upregulation of
353 HsAQP3 in a *P. berghei* dual RNAseq study (this was confirmed in our dataset, p = $1.81\text{x}10^{-19}$)

and also showed that this transporter is localized to the PVM[40]. Normally HsAQP3, a membrane transporter of water and glycerol, would be trafficked to the human cell plasma membrane. The host autophagosome marker, LC3, as well as other autophagosome markers, P62, NDP52, and NBR1 and LAMP1 also colocalize with UIS4[41-45]. The timing of relocalization is also similar, occurring here as early as 12 hours post infection, as observed for LC3[43]. While each protein that was examined here and by others could have a distinct role in supporting parasite development, we favor a model in which newly synthesized proteins are redirected to the vacuole and away from their natural home, potentially as a universal neutralization mechanism to block cell signaling and apoptosis in the infected host.

It has been proposed that one mechanism by which the malaria parasite may accomplish the host cell remodeling is through modification of the host autophagy pathways[46]. Here the host cell is relatively passive, and the parasite now directs the formation of lysosomes which are used to capture pieces of the host cytoplasm and redirect them toward the parasite. This has been termed the *Plasmodium*-associated autophagy-related (PAAR) response[46]. Support for this model comes from the demonstration that many autophagosome markers colocalize with the PVM and some are also needed for parasite development[46]. However, this does not explain why a variety of completely unrelated proteins, including MUC13, AQP3[40], NR4A3 or CXCL2, all show the same behavior. This model, which is based on what is observed in infected erythrocytes, does not necessarily take into account the massive transcriptional changes which are observed in infected hepatocytes. This autophagy model also suggests that lysosome cargo that is directed to the PV consists of digested proteins.

We propose an alternative but possibly complementary model in which newly synthesized host proteins are now secreted into the PV because the host secretion apparatus has been extensively modified. This model is supported by the fact that many of the antibodies we have used in our study are to full length proteins and their appearance in the PVR is associated with their transcriptional upregulation in the infected host cells. Our model is also based on our micrographs as well as those of others[47-49] showing that the endoplasmic reticulum (ER) is also relocalized to the PVR. In fact, the upregulation and association of HsGOLGA8A with the PVR may be a consequence of the relocalization of the ER and Golgi apparatus around the PV and may

be the easiest to understand in light of recent reports showing that the Golgi and ER move from around the host nucleus in uninfected cells to around the parasite[47-49].

Most of the proteins that we examined bear signal sequences that would direct them to the ER and Golgi. On the other hand, HsNR4A3, which presumably does not bear a signal sequence, would normally be translated in the cytoplasm and imported to the nucleus via the nuclear pore complex (NPC) by virtue of its nuclear localization signal. In early stages of the infection, HsNR4A3 is found in the nucleus and only later relocates to the PV. Do nuclear pore proteins somehow relocate from the nuclear membrane to the PVM? It is possible that nuclear pore complex proteins find their way to the PVM, as well. It was recently shown that infection with LS parasites results in the host microtubule organizing center (MTOC) relocalizing to the PVM. The authors of the paper suggested that during infection MTOCs reorganize the host microtubule network around the developing LS parasites[50]. It may be that there is an active contact site between the host nucleus and the PVM through the NPCs. Active contact sites between nucleus and mitochondria[51] or multiple inter-organelle contact sites[52] have been shown in mammalian cells.

Despite questions about how it occurs, the redirection of transcription factors away from the host nucleus into to the PV could provide physiological advantages to the parasite. It could render the infected cell less able to transcriptionally respond to external stimuli such as signals to divide, differentiate, or undergo apoptosis, all of which would likely be unfortunate events for the parasite. This could be particularly important for cells that must harbor hypnozoites for many years. The redirection of HsNR4A3 away from the nucleus could also have consequences for immune evasion. Proliferation and IL-2 production levels of T cells cocultured with HsNR4A3 knocked-down DCs were significantly lower than that of T cells cocultured with control DCs[53].

In contrast, HsCGA, HsMUC13, and HsCXCL2 are all secreted proteins (one membrane localized and two not) and would presumably be trafficked via the endoplasmic reticulum to the Golgi apparatus where they would be packaged into secretory vesicles for export. Further work and mutagenesis of reporters may be needed to determine whether there are specific signals that result in export to the PVM or PV.

The redirection of secretory vesicles to the PV versus to the extracellular space or cell membrane in infected cells could have strong immunological consequences. A number of human

412 cytokines and proteins from the fever-causing NLRP3 inflammasome[54] including ATM, CDCA8,
413 CXCL10, CXCL2, ESPL1, H2AFX, HMOX1, LIG1, MDM2, NFKBIE, OGG1, PRIM1, PTTG1,
414 RAD50, RAD51, RELB, TDP1, TP53, TYMS, and XRCC1 are differentially regulated in late
415 infected hepatocytes via pathway analysis (p = 0.0093) and the redirection of secreted proteins to
416 the PV could be a mechanism to both improve parasite nutrition and evade host immune responses.
417 The antigens that would normally be displayed on the major histocompatibility complex on the
418 infected hepatocyte cell surface and present parasite antigens to T cells are now being secreted into
419 the PV space, where they cannot be recognized by CD8+ T cells.

420 Although both infected and uninfected cells were treated identically in our expression
421 dataset, the use flow sorted hepatoma cells, could create artefactual patterns. Recently a single cell
422 RNA-seq study was published[55]. Although a comprehensive comparison of the mouse and human
423 transcriptomes is outside the scope of this study, the patterns in our cell culture dual RNAseq
424 dataset are supported by single RNA-seq data from mouse liver infected with *P. berghei*. In
425 general, both datasets showed upregulation of genes involved in immune modulation and
426 decreased expression of metabolism associated genes. The single cell mouse study shows that
427 MmNR4A3 is clearly upregulated in infected mouse hepatocytes (q = 9.18928E-06) as is
428 MmCXCL2 (q = 0).

429 The reason for clinical silence of the malaria parasite infected liver cells has long been a
430 source of discussion. Bertolino and Bowen speculated that one reason CD8+ T cells poorly
431 recognize infected hepatocytes in a natural infection is because of either the low numbers of
432 infected hepatocytes, or because of natural tolerance[56]. An alternative explanation is that secretion
433 is modified in infected cells to direct products to the PV, as supported by our data. Our data may
434 also explain why irradiated sporozoites, which can complete the early stages of invasion but do
435 not progress to liver schizonts could create a better immune response. It would be interesting to
436 evaluate the distribution of organellar markers such as HsBiP, and HsGOLGA8A with irradiated
437 sporozoites.

438 How the parasite accomplishes host cell remodeling is unknown. Our data support the
439 Golgi as key to host cell remodeling. Much of the Golgi structure and function is controlled by
440 small Rab GTPases, which are key regulators of intracellular transport and membrane trafficking

441 in eukaryotic cells GTPases[57]; De Niz et al. demonstrated the functional importance of the
442 GTPases ARF1 and RAB1A, in *P. berghei* exoerythrocytic stage development, when they
443 expressed dominant negatives (with gain-of-function mutations in the nucleotide binding sites)
444 and showed that these mutants proteins caused an arrest and lower survival of the parasite in HeLa
445 cells[48]. In the related apicomplexan parasite, *T. gondii*, genetic screens have shown that the parasite
446 releases effector molecules into the host cell cytoplasm when it invades[58]. Although parasite
447 proteins that are needed for exoerythrocytic stages to develop have been identified in genome wide
448 genetic screens[59], it is not clear which of these are released into the host cell cytoplasm and which
449 are retained within the parasite. Screens of these mutants using host markers will likely be needed
450 to identify these factors.

451 One of the most interesting discoveries is that host cell remodeling is also observed in *P.*
452 *vivax* hypnozoites, as this now presents a way to disturb the PV and potentially provide a radical
453 cure. *P. vivax* hypnozoites, which presumably are not replicating their DNA and are not growing,
454 have traditionally been challenging to eliminate. The 8-aminoquinoline family of compounds that
455 can eliminate hypnozoites were discovered by injecting hundreds of macaques with random
456 compounds and testing to see which were permanently cured of malaria[60,61]. Recently, phenotypic
457 screening systems have begun to identify other types of compounds that are critical to hypnozoite
458 survival[62]. Our work shows that early-stage *P. berghei*, and *P. vivax* EEFs both redirect
459 upregulated proteins to the PVR, and this presents a way to study the process. This could
460 potentially lead to the identification of drug targets for the elusive hypnozoite.

461

462

463

464

465

466

467

MATERIALS AND METHODS

Note: Requests for materials should be addressed to Elizabeth A. Winzeler: ewinzeler@health.ucsd.edu

Parasites

P. berghei-ANKA-GFP-Luc-SMCON (*Pb*-Luc)[63] and *P. berghei*-GFP (*Pb*-GFP)[63] sporozoites were obtained by dissection of infected *Anopheles stephensi*[64,65] mosquito salivary glands. Dissected salivary glands were homogenized in a glass tissue grinder and filtered twice through nylon cell strainers (20µm pore size, Millipore SCNY00020) and counted using a Neubauer hemocytometer. The sporozoites were kept on ice until needed. *Pb*-Luc and *Pb*-GFP-infected *An. stephensi* mosquitoes were also obtained from the Insectary Core Facility at New York University or from the Sporocore at the University of Georgia, Athens (Grant number R01 AI090141-08).

For *Pb*-Luc sporozoite production, female 6–8-week-old *Swiss webster* mice (UCSD Vivarium) were injected with blood stage *Pb*-Luc parasites to begin the growth cycle. Animal handling was conducted according to the UCSD Institutional Animal Care and Use Committee-approved protocols. *An. stephensi* mosquitoes raised at UCSD insectary were allowed to feed on infected mice with gametocytemia of ~10%. Dissected thorax sporozoites were isolated using a standard protocol at day 14 or 15 post-blood meal. The sporozoites were washed with DMEM incomplete media to remove debris from the thorax. The sporozoites were centrifuged 15,000 × g for 5 min at 4°C to pellet and resuspended in the desired volume of complete medium.

P. falciparum sporozoites strain NF54 were isolated from infected *An. stephensi* mosquito salivary glands. The sporozoites were isolated at TropIQ Health Sciences. Transistorweg 5, The Netheherlands.

Cell culture

HC-04[66], Huh7.5.1[67] and HepG2-A16-CD81^{EGFP} [68,69] cells were cultured at 37°C with 5% CO_2 in complete media (DMEM (Invitrogen, Carlsbad, USA) supplemented with 10% FBS, 0.29mg/mL glutamine, 100 units of penicillin, and 100µg/mL streptomycin). During and after the infection with *Pb*-Luc, or *Pb*-GFP, or *P. vivax* sporozoites, complete DMEM media was

supplemented with antibiotics 50µg/mL gentamycin, 50µg/mL neomycin, 100 units of penicillin, and 100µg/mL streptomycin, also antimycotics 50µg/mL 5-fluorocytosine, 100µg/mL posaconazole and 100µg/mL neomyxin. All cell lines and source are described in Table S1.

Infection of hepatocytes for qRT-PCR

Hepatocytes were seeded into 24-well plates (120,000 cells per well) 24h before infection, and infected with *Pb*-GFP sporozoites obtained from freshly dissected and infected *An. stephensi* mosquitoes at a ratio of 0.3 sporozoites per seeded cell. Plates were centrifuged at 330 × g for 3 min to bring sporozoites closer to cells, and plates were then incubated at 37°C in 5% CO_2 for 2h to promote sporozoite invasion[70]. After 2h, the cells were washed, fresh complete DMEM media were supplemented with 12µM 5-fluorocytosine (Cayman, #11635), 50µg/mL gentamicin sulfate (Gibco, #15710072), and 100µg/mL neomycin trisulfate salt hydrate (Sigma-Aldrich, #72133), and the cells were returned to the incubator.

Separation of infected and uninfected hepatocytes, RNA isolation and gene expression quantification by qRT-PCR

HepG2, Huh7.5.1 and HC-04 cells, in addition to primary human hepatocytes, were dissociated from plates at time zero (uninfected hepatocytes and sporozoites before infection), 24 and 48hpi by the addition of 500µL TrypLE Express (1×, ThermoFisher, #12605010), washed once using 1× PBS (Gibco, #14190144) and resuspended in FACS buffer (1× PBS supplemented with 1mM EDTA, 25mM HEPES and 0.5%FBS), then passed through a 40µm cell strainer prior to sorting (BD Falcon). Uninfected and infected cells were isolated by FACS using a BD Influx cell sorter with GFP mean fluorescence intensity (MFI) used to determine infection status. Overall gating strategy is as previously reported[17], and shown in Fig. S11 with total cells identified via Forward Scatter (FSC) vs Side Scatter (SSC) (P1 gate), individual cells identified via tandem gating of FSC-Height vs FSC-width and SSC-Height vs SSC-Width (gates P2 and P3), then GFP positive and negative cells were collected as indicated (gates P4, and P5 respectively). For RNA extraction, cells were directly sorted into Eppendorf tubes containing 600µL Qiazol reagent (Qiagen) and total RNA was extracted using the Qiagen miRNEasy Mini kit (Qiagen, #217004) according to manufacturer's instructions. Gene expression differences were measured using SYBR green qRT-PCR with PerfeCTa SYBR® Green FastMix (Quanta Bio, #95054), using the primers

indicated in Table S2, and a Bio-Rad CFX96 qRT-PCR system (Bio-Rad). Changes were quantitated according to the ΔΔCT method and normalized using Human Beta-2-Microglobulin (*B2M*) gene.

Dual RNA-sequencing analysis and code availability

We analyzed the gene differential expression using data previously generated and obtained in our group[17]. Reads can be found in the short read archive (http://www.ncbi.nlm.nih.gov/sra), under accession number PRJNA390648. We took the dual RNA-seq read count tables from the same study, and used DESeq2[71] with a multifactorial design, to calculate gene differential expression at both 24 and 48h for infected versus uninfected cells, in HepG2s, Huh7.5.1s and HC-04s cell lines as well as using HC-04 cells alone.

Determination of infection in hepatocytes through RNA quantification by qRT-PCR

Quantification of *Pb*-Luc infection was as previously described[72]. Briefly, 90,000 HC-04 HsNR4A3 WT and CRISPR/*Cas*9 edited cells were plated 24h before infection in 24-well plates. *Pb*-Luc parasites were added at a 1:2 ratio and complete DMEM media was changed 2h later. After 48h, infected cells were harvested and washed gently with PBS. RNA was isolated using Qiagen miRNEasy Mini Kit (Qiagen, #217004) according to manufacture instructions. RNA was quantified using a Nanodrop (Thermo Scientific) and cDNAs were synthetized using SuperScript™ II Reverse Transcriptase kit (Invitrogen, #18064022). Gene expression levels for parasite 18S RNA were then assessed by SYBR green qRT-PCR using perfecta SYBR Green FastMix (Applied Biosystems, #4367659), the set of primers described in Table S2, a Bio-Rad CFX Real-Time PCR system and quantitated using the ΔΔCT method and normalized against Human Hypoxanthine phosphoribosyltransferase 1 (*HPRT1*) gene.

Western blot of CRISPR/Cas9 edited cell lines

Cells were first plated, infected, and sorted for GFP as described above. After sorting, 1,000 infected or 150,000 uninfected cells were washed twice with cold 1× PBS. Cells were lysed via the addition of 200µL RIPA buffer (Teknova, #R3792) plus 1:100 protease inhibitor (Halt – Thermo Fisher Scientific, #78429). Equal numbers of cells were loaded onto the gel in 2× Laemmli Buffer (BioRad, #1610737), and proteins were loaded onto 18-well BioRad anyKD Criterion TGX gels (Bio-Rad, #5671124). For validation of HsNR4A3 protein knockout, 10µg of protein from

554 uninfected HC-04 WT and CRISPR/*Cas*9 edited cell lines were lysed in RIPA buffer as above and
555 loaded into identical gels.

556 Approach 1: Proteins were transferred to membranes and were probed with α-HsNR4A3
557 (dilution 1:100; HsNR4A3-Ab1), and α-HsVinculin (dilution 1:100; #ab129002) antibodies
558 overnight at 4°C, probed with goat α-mouse HRP (dilution 1:5,000; #7076P2) and goat α-rabbit
559 HRP secondary (dilution 1:5,000; #G-21234) respectively, and detected using Super Signal West
560 Pico, and Femto Chemiluminescent Substrate (Thermo Fisher, #34577 and #34090). Densitometry
561 was calculated using ImageJ (http://rsbweb.nih.gov/ij/) after image inversion and is shown relative
562 to loading control.

563 Approach 2: Proteins were transferred to membranes and were probed with α-HsNR4A3
564 (dilution 1:100; HsNR4A3-Ab1), and α-HsVinculin (dilution 1:100; #4650S) antibodies overnight
565 at 4°C, probed with goat α-mouse HRP secondary (dilution 1:5,000; #7076P2) or goat α-rabbit
566 HRP secondary (dilution 1:5,000; #7074S), and detected using SuperSignal West Pico and Femto
567 Chemiluminescent Substrate (Thermo Fisher, #34577 and #34095), images were acquired using a
568 gel documentation and analysis system (Syngene, G:Box) and the software Gen Sys V.1.4.3.0.
569 Densitometry was calculated using ImageJ (http://rsbweb.nih.gov/ij/) after image inversion and is
570 shown relative to loading control.

571 *Plasmodium exoerythrocytic form (EEF) culture for cellular localization*

572 For *Pb*-Luc imaging, 96-well glass bottom plates (MatTek Corporation) or 8-well Nunc
573 Lab-Tek slides (Thermo Scientific, #125658) were coated with Poly-L-Lysine 0.01% (v/v)
574 (Sigma, #P4707) and subsequently seeded with HC-04 cells (2,500 or 25,000 cells per well,
575 respectively) 24h before infection. *Pb*-Luc sporozoites were freshly isolated from infected *An.*
576 *stephensi* mosquitoes as above and resuspended in screening DMEM media (DMEM media
577 supplemented with 5% FBS, 1.46mg/mL glutamine, 500 units of penicillin, and 500µg/mL
578 streptomycin), and additionally we added 0.5µM posaconazole (Cayman), 12µM 5-fluorocytosine
579 (Cayman), 50µg/mL gentamicin sulfate (Gemini Bio-Products), and 100µg/mL neomycin
580 trisulfate salt hydrate (Sigma-Aldrich). Pre-seeded well plates were infected with *Pb*-Luc
581 sporozoites using a 1:2 infection ratio (sporozoite to cell) and incubated for 2h at 37°C in 5% CO_2.
582 After 2h infection, medium was replaced, and plates were incubated for 48h.

583 *P. falciparum experiments*

584 Sixty thousand human primary hepatocytes were seeded in 60 wells of a collagen-coated
585 96-well microtiter plate. Two days after seeding, cells were infected with fifty thousand
586 sporozoites of *Plasmodium falciparum* strain NF54 (isolated from infected *An. Stephensi*
587 mosquitos). Five days post-infection, cells were fixed with methanol, permeabilized, blocked,
588 incubated with different primary antibodies, and evaluated by immunofluorescence and confocal
589 microscopy.

590 *P. vivax experiments*

591 *P. vivax* sporozoites were isolated from infected *An. darlingi* mosquitoes from a laboratory-
592 established colony in the Peruvian Amazon region[73,74]. Briefly, 30 patients (18 years and older)
593 from the Iquitos region, who were diagnosed with *P. vivax* malaria by blood smear and who had
594 not received treatment yet were enrolled. Approximately 20mL of whole blood was collected.
595 After centrifugation at 500 × *g* for 5 min at 37°C, plasma was removed from the *P. vivax*-infected
596 packed red cells and replaced with an equal volume of heat inactivated O^+ plasma. Then the red
597 cells were used to feed fasted female *An. darlingi* mosquitoes using a standard membrane feeding
598 assay as previously described[73,74]. After seven days, a group of ten mosquitos were midgut
599 dissected and stained by mercurochrome to evaluate oocyst development, and 14 days after the
600 first infection mosquitoes were dissected to obtain sporozoites. Dissected salivary glands were
601 homogenized in a 1.5mL tube, crushed with a homogenizer, filtered twice using nylon cell strainers
602 (20µm pore size, Millipore SCNY00020), centrifuged, and resuspended in a 500µL final volume.
603 The number of sporozoites were counted using Neubauer hematocytometer. The sporozoites were
604 kept on ice until needed.

605 For Western blot assays, 6-well glass bottom plates (Thermo Scientific, #NUNC-140675)
606 were coated with Poly-L-Lysine 0.01% (v/v) (Sigma, #P4707) and seeded with HC-04 WT cells
607 (800,000 cells per well) 24h before *P. berghei* or *P. falciparum* NF54 sporozoites infection
608 (400,000 sporozoites per well). *P. berghei* or *P. falciparum* NF54 were diluted in DMEM media
609 using 1:2 infection ratio (sporozoites to HC-04 cells) and incubated 4h at 37°C under 5% CO_2
610 atmosphere. After this initial incubation period, infection media was replaced with fresh screening
611 DMEM media, plates with HC-04 cells infected with *P. berghei* were incubated for two days, and

612 the plates with HC-04 cells infected with *P. falciparum* were incubated for five days, the screening
613 DMEM media was replaced every 24h.

614 Uninfected and infected cells were lysed via the addition of 200µL RIPA buffer (Fisher
615 Scientific, #P189900) plus protease inhibitor cocktail (cOmplete Mini, EDTA-free – Roche,
616 #11836170001). Proteins (50µg) were mixed with 4× Laemmli Buffer (BioRad, #1610737), and
617 loaded onto 12-well BioRad Criterion TGX gels (Bio-Rad, #5671083). Proteins were transferred
618 to nitrocellulose membranes and were different primary antibodies overnight at 4°C (Table S2),
619 probed with goat α-mouse HRP secondary antibody (dilution 1:2,000; #7076P2), goat α-rabbit
620 HRP secondary antibody (dilution 1:2,000; #7074S) or rabbit α-goat HRP secondary antibody
621 (dilution 1:2,000; #A27014), and detected using SuperSignal West Pico or Femto
622 Chemiluminescent Substrate (Thermo Fisher, #34577 and #34095), images were acquired using a
623 gel documentation and analysis system (Syngene, G:Box) and the software Gen Sys V.1.4.3.0.

624 For IFA analysis 96-well glass bottom plates (MatTek Corporation) or 8-well Nunc Lab-
625 Tek chamber slides (Thermo Scientific, #125658) were coated with Poly-L-Lysine 0.01% (v/v)
626 (Sigma, #P4707) and seeded with HC-04 WT or CRISPR/*Cas*9 edited cells (2,500 or 25,000 cells
627 per well) 24h prior to mosquito dissection and infection. *P. vivax* sporozoites were diluted in
628 screening DMEM media (supplemented as above). Slides were infected using a 1:2 infection ratio
629 (sporozoites to HC-04 cells) and incubated for 4h at 37°C under 5% CO_2 atmosphere. After this
630 initial incubation period, infection media was replaced with fresh screening DMEM media, and
631 plates or slides were incubated for five days, the screening DMEM media was replaced every 24h.

632 *Plasmodium EEF and HsNR4A3 immunofluorescence microscopy and high content imaging*

633 All primary and secondary antibodies used in this study are given in Table S3-S5. We used
634 HC-04 HsNR4A3 wild type cells (HC-04 wild type), CRISPR/*Cas*9 edited cells lines (NM1, NM2
635 and NM3 or GL1, and GL3) and the *Pb*-Luc parasites[75]. The different cells lines were seeded in
636 8-well chamber slides and infected them with a 1:2 infection ratio (sporozoite to HC-04 cell). After
637 48h of infection, cells were fixed with 4% paraformaldehyde-PBS (Affymetrix, #19943) for 20
638 min at RT, permeabilized with 0.1% TritonX-100 (Fisher, #BP151500) for 10 min at RT, blocked
639 with 1% BSA for 1h and incubated with two antibodies overnight at 4°C. The first antibody was a
640 α-PvUIS4 or α-PbUIS4 (mouse monoclonal antibody for *P. vivax* UIS4 or goat polyclonal

antibody for *P. berghei* UIS4; dilution 1:500; α-PvUIS4 antibody donated by Kappe's Lab or α-PbUIS4 antibody, #LS-C204260), and for human host proteins the following set of antibodies were used: α-HsNR4A3 (dilution 1:100; HsNR4A3-Ab1), α-HsCGA (dilution 1:50; HsCGA-Ab1), α-HsGOLGA8A (dilution 1:50; HsGOLGA8A-Ab1), or α-HsMUC13 (dilution 1:50, HsMUC13-Ab1). Then, the following secondary antibodies were used for plasmodium parasites (PvUIS4 or PbUIS4) 1) Donkey α-mouse (dilution 1:1,000; #715297003) or bovine α-goat (dilution 1:1,000; #805297008), Rhodamine Red™-X - Red, and for the human host proteins: 2) Donkey α-mouse or goat α-rabbit (dilution 1:1,000; #A32766, or #111545046, Alexa Fluor 488 - Green) and incubated for 2h at RT. Hepatocyte plasma membrane was detected using CellMask deep red (Thermo Fisher Scientific, #C10046) at 1×. After IFA, chambers were removed from *Pb*-Luc-infected Lab-Tek systems, slides were mounted with Vectashield with DAPI (Vector Labs, #H-1500) and #1.5 glass coverslips were affixed using nail polish. Images were acquired using a Zeiss LSM880 with Airyscan Confocal Microscope (63× Plan-Apochromat /1.4 NA DIC oil immersion objective); laser power was set to 3% for 405, 488, 561, and 640nm. The images were processed using the confocal ZEN software (Black edition, Zeiss). The level of colocalization between the two fluorescent proteins (α-PbUIS4/α-HsNR4A3, α-PvUIS4/α-HsCGA, α-PvUIS4/α-HsGOLGA8A, α-PvUIS4/α-HsMUC13, or α-PbUIS4/α-HsCXCL2 were determined by calculating the product of the difference from the mean (PDM) indicated a mean Pearson coefficient r (Pearson correlation coefficient - PCC) in PV, α-PbUIS4 or α-PvUIS4 was on channel A vs human host protein on channel B. The PCC were analyzed using Volocity 3D/4D rendering software for three identified objects from each of three biological replicates.

Ultrastructure Expansion Microscopy (U-ExM)

Clean coverslips (Fisher Scientific, #NC1129240) pretreated with poly-l-lysine for 1h at 37°C, washed with MilliQ water, dried, and placed in the wells of a 12-well plate, were used to seed human liver cells (HC-04 or Huh7.5.1 cells, 200,000) resuspended in 1ml of DMEM complete media and incubated at 37°C, 5% CO_2, for 24h. The infection was performed with *P. berghei* sporozoites (100,000) at ratio 2:1 (two cells to one parasite), incubated during 48h, 37°C, 5% CO_2. Supernatants were removed, and the cells were fixed with 1 mL of 4% PFA (EMS #15710)/PBS for 20 min at 37°C. then stored and shipped overnight to the Absalon laboratory at Indiana

University School of Medicine. At reception, coverslips were proceeded for expansion microscopy as described in Liffner and Absalon 2021[38]. Gels were incubated overnight with primary antibodies with the following dilution 1:250 for α-PbUIS4 (#LS-C204260), and 1:100 for α-HsNR4A3 (HsNR4A3-Ab1) at room temperature on a shaker. All secondary antibodies were diluted 1:500 in PBS (donkey anti-goat-Alexa 488, ThermoFisher Scientific #A-11055 and donkey anti-mouse-Alexa 555, ThermoFisher Scientific #A-31570), 1:250 for NHS ester-Alexa 405 (ThermoFisher Scientific #A7573) and 1:1000 for Sytox™ Deep red (ThermoFisher Scientific #S11380) and incubated room temperature on a shaker for 2h and 30 min. Staining with 1:1000 Bodipy-TR-Ceramide (ThermoFisher Scientific #D7540) required an additional overnight room temperature on a shaker.

For imaging, small sections of the larger gel were cut and gently dried before being placed into 35 mm #1.5 coverslips bottomed imaging dishes (Cellvis; Fisher Scientific #NC0409658) precoated with poly-D-lysine. The images were acquired using a Zeiss LSM900 AxioObserver microscope with Airyscan 2 detector, with 63x Plan-Apochromat (NA 1.4) objective lens. All images were acquired in multiplex mode 2 as Z-stacks with and XY pixel size 0.035 µm and a Z-step size of 0.13 µm, and processed using Zen Blue software (Version 3.5, Zeiss, Oberkochen, Germany).

High content imaging (HCI) of edited lines

HC-04[66] CRISPR/*Cas*9 edited cell lines were seeded in 384-well plates or 8-well Lab-Tek slides and infected with *Pb*-Luc parasites[63] at a ratio 2:1 (cells/sporozoites). After 48h cells were fixed, permeabilized, blocked and incubated with α-PbUIS4 (dilution 1:500; #LS-C204260) and α-HsNR4A3 (dilution 1:100; HsNR4A3-Ab1), and visualized using bovine α-goat (#805297008, Rhodamine Red) and donkey α-mouse (#A32766, Alexa Fluor 488 - Green) secondary antibodies. The data were acquired (image analysis) using a High Content Imaging System (Operetta®, PerkingElmer). PbUIS4 protein was detected using the 568 channel (excitation 560-580nm, emission 590-640nm), exposure time of 200ms, and height of 82µm. HsNR4A3 protein was detected using the 488 channel (excitation 460-490nm, emission 500-550nm) with exposure time 200ms and height 82µm. Plasma membranes were detected using the DRAQ5 channel (excitation 620-640nm, emission 650-760nm) with exposure time of 200ms and a height

699 80µm. Nuclei (DAPI) were detected using an excitation wavelength of 360-400nm, emission 410-
700 480nm, with exposure time at 200 milliseconds (ms), and a height 40µm.

701 To evaluate and determined the size of *P. berghei* schizonts forms we use a splitting
702 coefficient of 0.40; common threshold, 0.40, split factor 72.0; individual threshold, 0.50; contrast,
703 0.50. Schizonts were also evaluated using different sets for diameter: 5, 20, 30 and 40µm^2. The
704 images were captured using a 10× long WD/0.3 NA objective, 10× magnification, 10 fields, 1
705 plane and 1 time point.

706 *Cytokine HsCXCL2 stimulation with lipopolysaccharide (LPS)*

707 To evaluate the expression of human chemokine HsCXCL2 (GROß), *in vitro* infections
708 were performed using the human liver line HC-04 with *P. berghei* sporozoites in 8-well Lab-Tek
709 slides. Cells were stimulated by treatment with 1µg/mL lipopolysaccharide (LPS), from *E. coli*
710 O55: B5 (Sigma Aldrich, # L6529). Cells were treated with different periods of exposition to LPS
711 (2, 24 and 48hpi), fixed and collected for confocal microscopy. The expression and localization
712 of HsCXCL2 protein in HC-04 cells were visualized through the use of the α-HsCXCL2 primary
713 antibody (dilution 1:100; HsCXCL2-Ab1). *P. berghei* parasites were visualized α-PbUIS4
714 polyclonal antibody (dilution 1:500; #LS-C204260), and their respective secondary antibodies
715 (dilution 1:1,000; #711296152 and #705546147). Plasma membranes were detected using
716 CellMask deep red, and nucleus were stained with DAPI.

717 *HsNR4A3 CRISPR/Cas9 (Approach 1)*

718 HsNR4A3 was edited using a sequential two plasmid CRISPR/*Cas9* approach. First, HC-
719 04 cells expressing CAS9 were generated using lentivirus containing the EF1a-*Cas9*-2A-
720 Blasticidin Lenti plasmid (Sigma Aldrich, #LVCAS9BST-1EA). HC-04 cells were plated at a
721 density of 120,000 cells per well in three independent wells of a 24 well plate. Twenty-four hours
722 after plating, media was replaced with complete media (as above) plus 5µg/mL polybrene and viral
723 particles. Cas9 lentiviral particles were added at a multiplicity of infection (MOI) of 0.5, after
724 which cells were spun at 800 × g for 30 min, then incubated overnight at 37°C. The following day
725 media, was changed to complete media and cells were again incubated overnight at 37°C. The
726 next day, cells were selected for presence of the CAS9 plasmid using complete media plus
727 2.5µg/mL blasticidin (Thermo Fisher, #A1113903). After 14 days of selection, splitting as

required, cells were trypsinized and plated at an average density of one cell per well in a 96 well plate in complete media plus blasticidin as above. Once cells had regrown, wells were observed via microscopy to identify those wells which appeared to contain single colonies. CAS9 expression within clones was then confirmed via PCR.

Once CAS9 expressing HC-04 cells were established, gRNA targeting *HsNR4A3* was introduced via Lentivirus containing the LV04 U6-gRNA:hPGK-Puro-2A-BFP plasmid and a gRNA sequence specific for Human *HsNR4A3*. The DNA sequence targeted by the gRNA for *HsNR4A3* was CTGCAGCAGCCTGGTCAGTGGG (Sigma-Aldrich Sanger Clone ID HS5000010424). Cells were infected with virus and cultured overnight as above. The following day, cells were selected for presence of the gRNA plasmid using complete media plus 2.5µg/mL puromycin (Gibco, #A1113803) and 2.5µg/mL blasticidin. Clonal cell lines expressing the gRNA and CAS9 were generated as previously stated. The presence of *HsNR4A3* knockout within these apparent monoclonal HC-04 cell lines was examined at the protein level, after being expanded into 25cm^2 vented tissue culture flasks, via western blot using the HsNR4A3 rabbit polyclonal antibody (dilution 1:100; HsNR4A3-Ab1). Three edited clones (clones GL1, GL2, and GL3) were then examined using confocal microscopy, all exhibited low or no host cell HsNR4A3 protein expression.

HsNR4A3 CRISPR/Cas9 (Approach 2)

A second round of editing for *HsNR4A3* was performed using a single plasmid CRISPR/*Cas9* system with the Edit-R All-in-one Lentiviral an sgRNA, targeting *HsNR4A3*, packaged in a lentiviral vector (Horizon, Perkin Elmer). The gRNA sequence used was TTCGACGTCTCTTGTCTACT, targeting exon 5 of *HsNR4A3* coding sequence. Briefly, HC-04 cells were plated at a density of 150,000 cells per well in a 6 well plate, then 24h later media was replaced with complete media supplemented with 10µg/mL polybrene. Virus was added at a multiplicity of infection of one and then incubated overnight at 37°C. After 48h, the cells were selected for presence of the CAS9 plasmid using complete media plus 2.5µg/mL puromycin. After seven days of selection, cells were trypsinized and plated at an average density of 0.5 cell per well in a 96-well plate in the presence of 2.5µg/mL puromycin for clonal selection. After ~15-20 days, wells were observed via microscopy to identify those wells which contained single colonies. These

cells were then transferred to 6-well plates and the knockout of HsNR4A3 was confirmed in these apparent monoclonal HC-04 cell lines with immunoblotting.

Since, in the above obtained clones, there was only partial knockout of HsNR4A3, another round of transductions was performed using guide RNA GCTCGAGTAGCCCTCCACGA targeting at exon 4. Lenti-V2-Blast (lentiCRISPR v2-Blast plasmid, Addgene) plasmid was used here. Transductions were performed, as mentioned above, and the transformed cells were selected using 1µg/mL blasticidin and 2.5µg/mL puromycin. The clones obtained after clonal selection were evaluated for HsNR4A3 expression by immunoblotting using the HsNR4A3 mouse monoclonal antibody (dilution 1:100; HsNR4A3-Ab1). Three knockdown clones (clones NM1, NM2, and NM3) were selected to have low HsNR4A3 expression. These clones were then used for further studies.

ETHICS STATEMENT

Human subject protocols were approved by the Human Research Protection Program of the University of California, San Diego (approval number 120652) and Universidad Peruana Cayetano Heredia (approval number 102357). Written informed consent was obtained from all study participants.

ACKNOWLEDGMENTS

We thank the members of the Winzeler laboratory for advice and critical reading of the manuscript. In addition, we thank Medicines for Malaria Venture and Fogarty International Center of the National Institutes of Health (NIH) under Award Number D43TW009343 and the University of California Global Health Institute (UCGHI) for all their support of the insectary in Peru. We would also like to thank the UCSD Human Embryonic Stem Cell Flow Cytometry Core Facility, and UCSD Microscopy Core – NINDS NS047101 for their technical support. JC was supported by the Fogarty International Center of the National Institutes of Health (NIH) under Award Number D43TW009343 and the University of California Global Health Institute (UCGHI). GL was supported by an A.P. Giannini Post-Doctoral Fellowship. EAW is supported by grants from the NIH (1R01AI152533 and R01AI103058), and MMV. The *P. vivax* work was supported by

grants to JMV from the NIH (D43TW007120 and U19AI089681) and MMV. GTW was supported by NIH training grant T32AI007036. M.R. lab funded by the NIH grants AI126277, AI145325, AI154644, AI114625, by the Chiba University-University of California-San Diego (UCSD) Center for Mucosal Immunology, Allergy, and Vaccines, and by the UCSD Department of Pediatrics. M.R. also holds an Investigator in the Pathogenesis of Infectious Disease Award from the Burroughs Wellcome Fund.

AUTHOR CONTRIBUTIONS

JC performed Immunofluorescence, HCI, qRT-PCR, Western blot assays and data analysis. GL infected and sorted liver cells, isolated RNA for both infected and uninfected populations and measured gene expression levels via qRT-PCR and Western blot. JC and LG performed *P. vivax* liver stage assays. GL, BYZ, EP and NM generated *HsNR4A3* edited cell lines. JC, GL, and EW wrote the manuscript. KPGM analyzed data and created figures. BC contributed concepts and helped fund the study. CTR, DG and JV developed methods and infrastructure for *P. vivax* infections. GTW performed ELISA assays for HsCXCL2 protein. SA and BL performed U-ExM and imaging. All authors assisted with editing of the manuscript. The authors declare no conflicts of interest or competing financial interests.

REFERENCES

1 Fodor, S. P. *et al.* Multiplexed biochemical assays with biological chips. *Nature* **364**, 555-556 (1993).

2 Pradel, G. & Frevert, U. Malaria sporozoites actively enter and pass through rat Kupffer cells prior to hepatocyte invasion. *Hepatology* **33**, 1154-1165 (2001). https://doi.org:10.1053/jhep.2001.24237

3 Barnwell, J. W. Hepatic Kupffer cells: the portal that permits infection of hepatocytes by malarial sporozoites? *Hepatology* **33**, 1331-1333 (2001). https://doi.org:10.1053/jhep.2001.24740

4 Frischknecht, F. & Matuschewski, K. Plasmodium Sporozoite Biology. *Cold Spring Harb Perspect Med* **7** (2017). https://doi.org:10.1101/cshperspect.a025478

5 Mota, M. M., Hafalla, J. C. & Rodriguez, A. Migration through host cells activates Plasmodium sporozoites for infection. *Nat Med* **8**, 1318-1322 (2002). https://doi.org:10.1038/nm785

6 Sinai, A. *The Toxoplasma gondii Parasitophorous Vacuole Membrane: A multifunctional Organelle in the Infected Cell*. (2014).

7 Markus, M. B. Malaria: origin of the term "hypnozoite". *J Hist Biol* **44**, 781-786 (2011). https://doi.org:10.1007/s10739-010-9239-3

8 Vaughan, A. M. & Kappe, S. H. I. Malaria Parasite Liver Infection and Exoerythrocytic Biology. *Cold Spring Harb Perspect Med* **7** (2017). https://doi.org:10.1101/cshperspect.a025486

9 Wilby, K. J., Lau, T. T., Gilchrist, S. E. & Ensom, M. H. Mosquirix (RTS,S): a novel vaccine for the prevention of Plasmodium falciparum malaria. *Ann Pharmacother* **46**, 384-393 (2012). https://doi.org:10.1345/aph.1AQ634

10 Casares, S., Brumeanu, T. D. & Richie, T. L. The RTS,S malaria vaccine. *Vaccine* **28**, 4880-4894 (2010). https://doi.org:10.1016/j.vaccine.2010.05.033

11 Laurens, M. B. RTS,S/AS01 vaccine (Mosquirix?): an overview. *Human Vaccines & Immunotherapeutics* **16**, 480-489 (2020). https://doi.org:10.1080/21645515.2019.1669415

12 Nussenzweig, R., Vanderberg, J. & Most, H. Protective immunity produced by the injection of x-irradiated sporozoites of Plasmodium berghei. IV. Dose response, specificity and humoral immunity. *Mil Med* **134**, 1176-1182 (1969).

13 Sharma, S. & Pathak, S. Malaria vaccine: a current perspective. *J Vector Borne Dis* **45**, 1-20 (2008).

14 Goh, Y. S., McGuire, D. & Renia, L. Vaccination With Sporozoites: Models and Correlates of Protection. *Front Immunol* **10**, 1227 (2019). https://doi.org:10.3389/fimmu.2019.01227

15 Leiriao, P., Mota, M. M. & Rodriguez, A. Apoptotic Plasmodium-infected hepatocytes provide antigens to liver dendritic cells. *J Infect Dis* **191**, 1576-1581 (2005). https://doi.org:10.1086/429635

16 Vaughan, A. M., Wang, R. & Kappe, S. H. Genetically engineered, attenuated whole-cell vaccine approaches for malaria. *Hum Vaccin* **6**, 107-113 (2010). https://doi.org:10.4161/hv.6.1.9654

17 LaMonte, G. M. *et al.* Dual RNA-seq identifies human mucosal immunity protein Mucin-13 as a hallmark of Plasmodium exoerythrocytic infection. *Nat Commun* **10**, 488 (2019). https://doi.org:10.1038/s41467-019-08349-0

18 Mueller, A. K. *et al.* Plasmodium liver stage developmental arrest by depletion of a protein at the parasite-host interface. *Proc Natl Acad Sci U S A* **102**, 3022-3027 (2005). https://doi.org:10.1073/pnas.0408442102

19 Bertiaux, E. *et al.* Expansion microscopy provides new insights into the cytoskeleton of malaria parasites including the conservation of a conoid. *PLoS Biol* **19**, e3001020 (2021). https://doi.org:10.1371/journal.pbio.3001020

20 McGuckin, M. A., Linden, S. K., Sutton, P. & Florin, T. H. Mucin dynamics and enteric pathogens. *Nat Rev Microbiol* **9**, 265-278 (2011). https://doi.org:10.1038/nrmicro2538

21 Fu, Y., Luo, L., Luo, N., Zhu, X. & Garvey, W. T. NR4A orphan nuclear receptors modulate insulin action and the glucose transport system: potential role in insulin resistance. *J Biol Chem* **282**, 31525-31533 (2007). https://doi.org:10.1074/jbc.M701132200

22 Reynolds, M. S. *et al.* beta-Cell deletion of Nr4a1 and Nr4a3 nuclear receptors impedes mitochondrial respiration and insulin secretion. *Am J Physiol Endocrinol Metab* **311**, E186-201 (2016). https://doi.org:10.1152/ajpendo.00022.2016

23 Close, A. F., Dadheech, N., Villela, B. S., Rouillard, C. & Buteau, J. The orphan nuclear receptor Nor1/Nr4a3 is a negative regulator of beta-cell mass. *J Biol Chem* **294**, 4889-4897 (2019). https://doi.org:10.1074/jbc.RA118.005135

24 Duez, H. & Pourcet, B. Nuclear Receptors in the Control of the NLRP3 Inflammasome Pathway. *Front Endocrinol (Lausanne)* **12**, 630536 (2021). https://doi.org:10.3389/fendo.2021.630536

25 Fedorova, O. *et al.* Orphan receptor NR4A3 is a novel target of p53 that contributes to apoptosis. *Oncogene* **38**, 2108-2122 (2019). https://doi.org:10.1038/s41388-018-0566-8

26 Casarini, L., Santi, D., Brigante, G. & Simoni, M. Two Hormones for One Receptor: Evolution, Biochemistry, Actions, and Pathophysiology of LH and hCG. *Endocr Rev* **39**, 549-592 (2018). https://doi.org:10.1210/er.2018-00065

27 Bieche, I. *et al.* The CGA gene as new predictor of the response to endocrine therapy in ER alpha-positive postmenopausal breast cancer patients. *Oncogene* **20**, 6955-6959 (2001). https://doi.org:10.1038/sj.onc.1204739

28 Lu, P., Zhang, C. H., Lifshitz, L. M. & ZhuGe, R. Extraoral bitter taste receptors in health and disease. *J Gen Physiol* **149**, 181-197 (2017). https://doi.org:10.1085/jgp.201611637

29 Zhang, P., Cao, L., Zhou, R., Yang, X. & Wu, M. The lncRNA Neat1 promotes activation of inflammasomes in macrophages. *Nat Commun* **10**, 1495 (2019). https://doi.org:10.1038/s41467-019-09482-6

30 Kim, J. *et al.* Long noncoding RNA MALAT1 suppresses breast cancer metastasis. *Nat Genet* **50**, 1705-1715 (2018). https://doi.org:10.1038/s41588-018-0252-3

31 Menon, M. P. & Hua, K. F. The Long Non-coding RNAs: Paramount Regulators of the NLRP3 Inflammasome. *Front Immunol* **11**, 569524 (2020). https://doi.org:10.3389/fimmu.2020.569524

32 Liu, J. *et al.* The role of the Golgi apparatus in disease (Review). *Int J Mol Med* **47** (2021). https://doi.org:10.3892/ijmm.2021.4871

33 Gillingham, A. K. & Munro, S. Finding the Golgi: Golgin Coiled-Coil Proteins Show the Way. *Trends Cell Biol* **26**, 399-408 (2016). https://doi.org:10.1016/j.tcb.2016.02.005

34 Mikolajczak, S. A. *et al.* Plasmodium vivax liver stage development and hypnozoite persistence in human liver-chimeric mice. *Cell Host Microbe* **17**, 526-535 (2015). https://doi.org:10.1016/j.chom.2015.02.011

35 Nomiyama, T. *et al.* The NR4A orphan nuclear receptor NOR1 is induced by platelet-derived growth factor and mediates vascular smooth muscle cell proliferation. *J Biol Chem* **281**, 33467-33476 (2006). https://doi.org:10.1074/jbc.M603436200

36 Jakymiw, A. *et al.* Identification and characterization of a novel Golgi protein, golgin-67. *J Biol Chem* **275**, 4137-4144 (2000). https://doi.org:10.1074/jbc.275.6.4137

37 Friesen, J. *et al.* Natural immunization against malaria: causal prophylaxis with antibiotics. *Sci Transl Med* **2**, 40ra49 (2010). https://doi.org:2/40/40ra49 [pii]

10.1126/scitranslmed.3001058

38 Liffner, B. & Absalon, S. Expansion Microscopy Reveals Plasmodium falciparum Blood-Stage Parasites Undergo Anaphase with A Chromatin Bridge in the Absence of Mini-

Chromosome Maintenance Complex Binding Protein. *Microorganisms* **9** (2021). https://doi.org:10.3390/microorganisms9112306

39 De Filippo, K. *et al.* Mast cell and macrophage chemokines CXCL1/CXCL2 control the early stage of neutrophil recruitment during tissue inflammation. *Blood* **121**, 4930-4937 (2013). https://doi.org:10.1182/blood-2013-02-486217

40 Posfai, D. *et al.* Plasmodium parasite exploits host aquaporin-3 during liver stage malaria infection. *PLoS Pathog* **14**, e1007057 (2018). https://doi.org:10.1371/journal.ppat.1007057

41 Agop-Nersesian, C. *et al.* Shedding of host autophagic proteins from the parasitophorous vacuolar membrane of Plasmodium berghei. *Sci Rep* **7**, 2191 (2017). https://doi.org:10.1038/s41598-017-02156-7

42 Grutzke, J. *et al.* The spatiotemporal dynamics and membranous features of the Plasmodium liver stage tubovesicular network. *Traffic* **15**, 362-382 (2014). https://doi.org:10.1111/tra.12151

43 Real, E. *et al.* Plasmodium UIS3 sequesters host LC3 to avoid elimination by autophagy in hepatocytes. *Nat Microbiol* **3**, 17-25 (2018). https://doi.org:10.1038/s41564-017-0054-x

44 Schmuckli-Maurer, J. *et al.* Inverted recruitment of autophagy proteins to the Plasmodium berghei parasitophorous vacuole membrane. *PLoS One* **12**, e0183797 (2017). https://doi.org:10.1371/journal.pone.0183797

45 Niklaus, L. *et al.* Deciphering host lysosome-mediated elimination of Plasmodium berghei liver stage parasites. *Sci Rep* **9**, 7967 (2019). https://doi.org:10.1038/s41598-019-44449-z

46 Agop-Nersesian, C., Niklaus, L., Wacker, R. & Theo Heussler, V. Host cell cytosolic immune response during Plasmodium liver stage development. *FEMS Microbiol Rev* **42**, 324-334 (2018). https://doi.org:10.1093/femsre/fuy007

47 Bano, N., Romano, J. D., Jayabalasingham, B. & Coppens, I. Cellular interactions of Plasmodium liver stage with its host mammalian cell. *Int J Parasitol* **37**, 1329-1341 (2007). https://doi.org:10.1016/j.ijpara.2007.04.005

48 De Niz, M. *et al.* Hijacking of the host cell Golgi by Plasmodium berghei liver stage parasites. *J Cell Sci* **134** (2021). https://doi.org:10.1242/jcs.252213

49 Deschermeier, C. *et al.* Mitochondrial lipoic acid scavenging is essential for Plasmodium berghei liver stage development. *Cell Microbiol* **14**, 416-430 (2012). https://doi.org:10.1111/j.1462-5822.2011.01729.x

50 Vijayan, K. *et al.* A genome-wide CRISPR-Cas9 screen identifies CENPJ as a host regulator of altered microtubule organization during Plasmodium liver infection. *Cell Chem Biol* **29**, 1419-1433 e1415 (2022). https://doi.org:10.1016/j.chembiol.2022.06.001

51 Eisenberg-Bord, M. *et al.* Cnm1 mediates nucleus-mitochondria contact site formation in response to phospholipid levels. *J Cell Biol* **220** (2021). https://doi.org:10.1083/jcb.202104100

52 Kakimoto, Y. *et al.* Visualizing multiple inter-organelle contact sites using the organelle-targeted split-GFP system. *Sci Rep* **8**, 6175 (2018). https://doi.org:10.1038/s41598-018-24466-0

53 Nagaoka, M. *et al.* The Orphan Nuclear Receptor NR4A3 Is Involved in the Function of Dendritic Cells. *J Immunol* **199**, 2958-2967 (2017). https://doi.org:10.4049/jimmunol.1601911

54 Swanson, K. V., Deng, M. & Ting, J. P. The NLRP3 inflammasome: molecular activation and regulation to therapeutics. *Nat Rev Immunol* **19**, 477-489 (2019). https://doi.org:10.1038/s41577-019-0165-0

55 Afriat, A. *et al.* A spatiotemporally resolved single-cell atlas of the Plasmodium liver stage. *Nature* **611**, 563-569 (2022). https://doi.org:10.1038/s41586-022-05406-5

56 Bertolino, P. & Bowen, D. G. Corrigendum: Malaria and the liver: immunological hide-and-seek or subversion of immunity from within? *Front Microbiol* **6**, 460 (2015). https://doi.org:10.3389/fmicb.2015.00460

57 Goud, B., Liu, S. & Storrie, B. Rab proteins as major determinants of the Golgi complex structure. *Small GTPases* **9**, 66-75 (2018). https://doi.org:10.1080/21541248.2017.1384087

58 Hunter, C. A. & Sibley, L. D. Modulation of innate immunity by Toxoplasma gondii virulence effectors. *Nat Rev Microbiol* **10**, 766-778 (2012). https://doi.org:10.1038/nrmicro2858

59 Stanway, R. R. *et al.* Genome-Scale Identification of Essential Metabolic Processes for Targeting the Plasmodium Liver Stage. *Cell* **179**, 1112-1128.e1126 (2019). https://doi.org:10.1016/j.cell.2019.10.030

60 Dow, G. S. *et al.* Radical curative efficacy of tafenoquine combination regimens in Plasmodium cynomolgi-infected Rhesus monkeys (Macaca mulatta). *Malar J* **10**, 212 (2011). https://doi.org:10.1186/1475-2875-10-212

61 Baird, J. K. 8-Aminoquinoline Therapy for Latent Malaria. *Clin Microbiol Rev* **32** (2019). https://doi.org:10.1128/CMR.00011-19

62 Roth, A. *et al.* A comprehensive model for assessment of liver stage therapies targeting Plasmodium vivax and Plasmodium falciparum. *Nat Commun* **9**, 1837 (2018). https://doi.org:10.1038/s41467-018-04221-9

63 Janse, C. J. *et al.* High efficiency transfection of Plasmodium berghei facilitates novel selection procedures. *Molecular and Biochemical Parasitology* **145**, 60-70 (2006). https://doi.org:10.1016/j.molbiopara.2005.09.007

64 Rosenberg, R., Wirtz, R. A., Schneider, I. & Burge, R. An estimation of the number of malaria sporozoites ejected by a feeding mosquito. *Trans R Soc Trop Med Hyg* **84**, 209-212 (1990). https://doi.org:10.1016/0035-9203(90)90258-g

65 Medica, D. L. & Sinnis, P. Quantitative dynamics of Plasmodium yoelii sporozoite transmission by infected anopheline mosquitoes. *Infect Immun* **73**, 4363-4369 (2005). https://doi.org:10.1128/IAI.73.7.4363-4369.2005

66 Sattabongkot, J. *et al.* Establishment of a human hepatocyte line that supports in vitro development of the exo-erythrocytic stages of the malaria parasites Plasmodium falciparum and P. vivax. *Am J Trop Med Hyg* **74**, 708-715 (2006).

67 Swann, J. *et al.* High-Throughput Luciferase-Based Assay for the Discovery of Therapeutics That Prevent Malaria. *ACS Infect Dis* **2**, 281-293 (2016). https://doi.org:10.1021/acsinfecdis.5b00143

68 Yalaoui, S. *et al.* Hepatocyte permissiveness to Plasmodium infection is conveyed by a short and structurally conserved region of the CD81 large extracellular domain. *PLoS Pathog* **4**, e1000010 (2008). https://doi.org:10.1371/journal.ppat.1000010

69 Silvie, O. *et al.* Expression of human CD81 differently affects host cell susceptibility to malaria sporozoites depending on the Plasmodium species. *Cell Microbiol* **8**, 1134-1146 (2006). https://doi.org:10.1111/j.1462-5822.2006.00697.x

70 Prudencio, M., Rodriguez, A. & Mota, M. M. The silent path to thousands of merozoites: the Plasmodium liver stage. *Nature reviews. Microbiology* **4**, 849-856 (2006). https://doi.org:10.1038/nrmicro1529

71 Love, M. I., Huber, W. & Anders, S. Moderated estimation of fold change and dispersion for RNA-seq data with DESeq2. *Genome Biol* **15**, 550 (2014). https://doi.org:10.1186/s13059-014-0550-8

72 Bahamontes-Rosa, N. *et al.* New molecular settings to support in vivo anti-malarial assays. *Malar J* **15**, 147 (2016). https://doi.org:10.1186/s12936-016-1205-x

73 Moreno, M. *et al.* Infection of laboratory-colonized Anopheles darlingi mosquitoes by Plasmodium vivax. *Am J Trop Med Hyg* **90**, 612-616 (2014). https://doi.org:10.4269/ajtmh.13-0708

74 Moreno, M. *et al.* Continuous Supply of Plasmodium vivax Sporozoites from Colonized Anopheles darlingi in the Peruvian Amazon. *ACS Infect Dis* **4**, 541-548 (2018). https://doi.org:10.1021/acsinfecdis.7b00195

75 Franke-Fayard, B. *et al.* Simple and sensitive antimalarial drug screening in vitro and in vivo using transgenic luciferase expressing Plasmodium berghei parasites. *Int J Parasitol* **38**, 1651-1662 (2008). https://doi.org:10.1016/j.ijpara.2008.05.012

FIGURE LEGENDS

Figure 1. ***HsNR4A3* is highly upregulated during *Plasmodium* exoerythrocytic infection. a.** Schematic representation for culture, sorting by FACs, dual RNA Seq and confocal microscopy strategies, **b.** Volcano plot of differently expressed genes, gene-expression pattern vs *p* value, with the position of *HsMUC13, HsCGA, HsSLC22A8, HsMALAT1, HsRASSF9, HsSDHA, HsSLC25A27, HsNEAT1, HsTAS2R4*, *HsCXCL2,* and *HsNR4A3* genes indicated at 24 and 48hpi. **c.** RT-qPCR of *HsMUC13, HsCGA, HsSLC22A8, HsMALAT1, HsRASSF9, HsSDHA, HsSLC25A27, HsNEAT1, HsTAS2R4,* and *HsNR4A3* at 48hpi in the indicated cell lines. *HsSDHA* was used as a control. Relative quantitation of the indicated host transcripts calculated using ΔΔCT method, in the indicated hepatocyte cell types (data presented as mean ± s.e.m, *n*=3 with individual biological replicates overlaid, * = *p* value 0.05, ** = *p* value 0.001, *** = *p* value 0.0001, **** = *p* value <0.0001. *p* values determined by two-tailed *t* test). Data from LaMonte et al.[17].

Edited version—please check very carefully, especially for colors, which don't make sense.

Figure 2. Immunofluorescence micrographs of *Plasmodium*-infected cells using antibodies to HsNR4A3, HsCGA, HsGOLGA8A, and HsMUC13. Shown are representative confocal microscopy images of: **a.** HC-04 liver cells infected with *P. berghei* parasites 48hpi; **b.** primary hepatocytes infected with *P. falciparum* parasites 120hpi; **c.** HC-04 liver cells infected with *P. vivax* schizonts 120hpi; and **d.** HC-04 liver cells infected with *P. vivax* hypnozoites (white filled arrowheads) 120hpi. Parasites were visualized with a goat-α-PbUIS4 (#LS-C204260) (panels a, b, a1, a2, a3) or a mouse-α-PvUIS4 (panel c, d, d1) primary and bovine-α-goat (#805297008, Rhodamine Red (panels a, b)) or donkey-α-mouse (#715297003, Rhodamine Red (panels c, d)) secondary antibodies. Membranes were stained with CellMask deep red (magenta) and nuclei were labeled with DAPI (blue). Primary and secondary antibody combinations for human proteins (green) were as follows: mouse α-HsNR4A3 (HsNR4A3-Ab1) and donkey α-mouse (#A32766, Alexa Fluor 488 - Green); rabbit α-HsCGA (HsCGA-Ab1), rabbit α-HsGOLGA8A (HsGOLGA8A-Ab1), or rabbit α-HsMUC13 (HsMUC13-Ab1) primary antibodies and goat-α-rabbit (#111545046, Alexa Fluor 488 – Green) secondary antibodies. For a-d, scale bars are 10μm. In the DAPI (blue) panel, the infected (I) and uninfected (UI) cells are

labeled. Parasite nuclei (PN) and the host nucleus (HN) are shown (white filled arrows). Lower panels show zooms and panoramic fields for NR4A3 stained as described above for *P. berghei* infected cells (a1, a2, a3) or *P. vivax* infected cells (d1). Golgi in uninfected HC-04 cells are show (Golgi-UI, white filled arrows on panel a). All images were taken with a 63× oil objective.

Figure 3: Time-dependent relocalization of HsNR4A3 protein in HC-04 cells infected with *P. berghei* parasites a. Micrographs show HC-04 cells uninfected (0h), and infected with *P. berghei* EEFs at different times (6, 12, 18, 24, 48, and 72hpi). Human host protein was labeled using a α-HsNR4A3 (HsNR4A3-Ab1) and visualized with a donkey α-mouse secondary antibody (#A32766, Alexa Fluor 488 – Green); *P. berghei* parasites were labeled using α-PbUIS4 (#LS-204260) antibody and visualized with a bovine α-goat secondary antibody (#805297008, Rhodamine red). CellMask deep red was used for plasma membranes (magenta). Nuclei were labeled with DAPI (blue). Merged images between HsNR4A3, PbUIS4, DAPI, and Cell Membrane are shown. Scale bars 10μm; 63× oil objective. Two micrographs show HC-04 cells infected with *P. berghei* parasites (48h) and labeled with a single primary antibody (α-PbUIS4 or HsNR4A3-Ab1). In the DAPI (nuclei) panels, the infected (I) and non-infected (UI) cells are labeled. Parasite nuclei (PN) and the host nucleus (HN) are also shown (pointed with white filled arrows). **b.** Schematic representation of HsNR4A3 relocalization during *Plasmodium* exoerythrocytic infection in infected liver cells.

Figure 4. U-ExM of Huh7.5.1 cells infected with *P. berghei* parasites shows HsNR4A3 protein at the PVM. Five representative micrographs show Huh7.5.1 cells 48hpi with *P. berghei* parasites prepared for U-ExM (see Methods), stained with a nuclear stain (Sytox Deep Red in cyan), α-PbUIS4 (in magenta), HsNR4A3-Ab1 (in yellow) and a protein stain (NHS-ester, in grayscale) and visualized using Airyscan 2 microscopy. Yellow arrows indicate concentration of HsNR4A3 in pockets associated with the PVM. Scale bars as labelled in each image, solid bar = XY scale and all images are Z-projections with a combined depth of slices of 0.39 μm.

Figure 5. Relocation of HsCXCL2 protein in HC-04 cells infected with *P. berghei* parasites in different periods (2, 24, and 48hpi). a. Representative immunofluorescence confocal micrographs show HC-04 cells infected with *P. berghei* parasites, treated with LPS (1μg/ml) using indicated time. Cells were labeled using rabbit-α-HsCXCL2 (HsCXCL2-Ab1) antibody and

visualized with a donkey α-rabbit secondary antibody (#711296152, Rhodamine red); CellMask deep red was used for plasma membranes (Cell Membrane - magenta). *P. berghei* parasites were labeled using a goat-α-PbUIS4 (#LS-204260) antibody and visualized with a donkey-α-goat secondary antibody (#705546147, Alexa Fluor 488 - Green). Nuclei were labeled with DAPI (blue) with the infected (I) and non-infected (UI) cells with parasite nuclei (PN) and the host nucleus (HN) also shown (white filled arrows). Scale bars 10μm; 63× oil objective. Single primary antibody labeling (α-PbUIS4 or HsCXCL2-Ab1) in infected and uninfected cells without (w/o) and with (w/) LPS treatment are shown. Scale bars 10μm; 63× oil objective. **b.** Pearson's correlation coefficient (PCC) between α-PvUIS4 and HsCXCL2-Ab1 staining. Images were analyzed with Volocity 3D/4D Rendering Software, and PCC was calculated for identified objects. Each point represents one infected cell from one of three biological replicates. Data were analyzed with a two-tailed *t* test, * = $p < 0.0112$, **** = $p < 0.0001$.

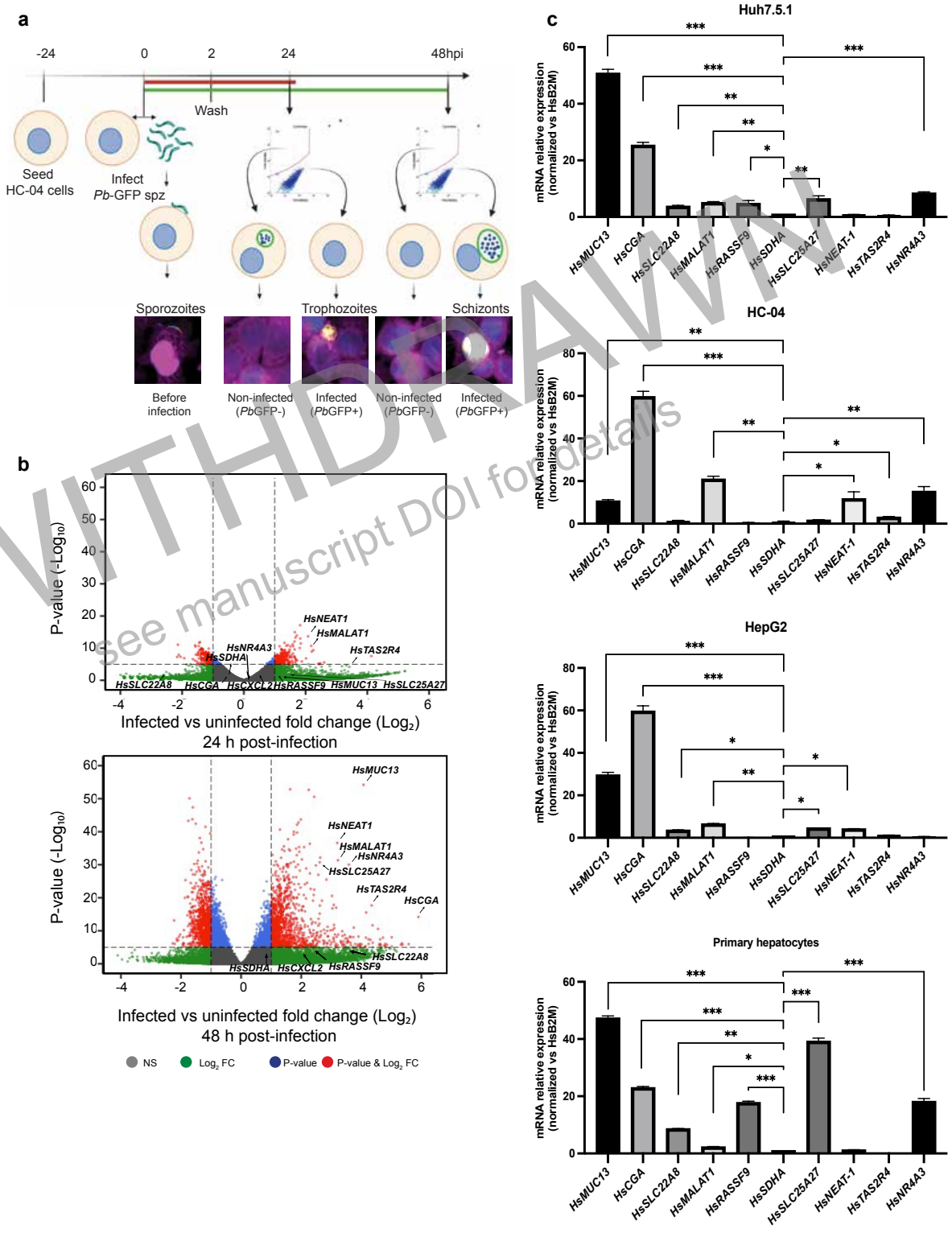

Figure 1

1129

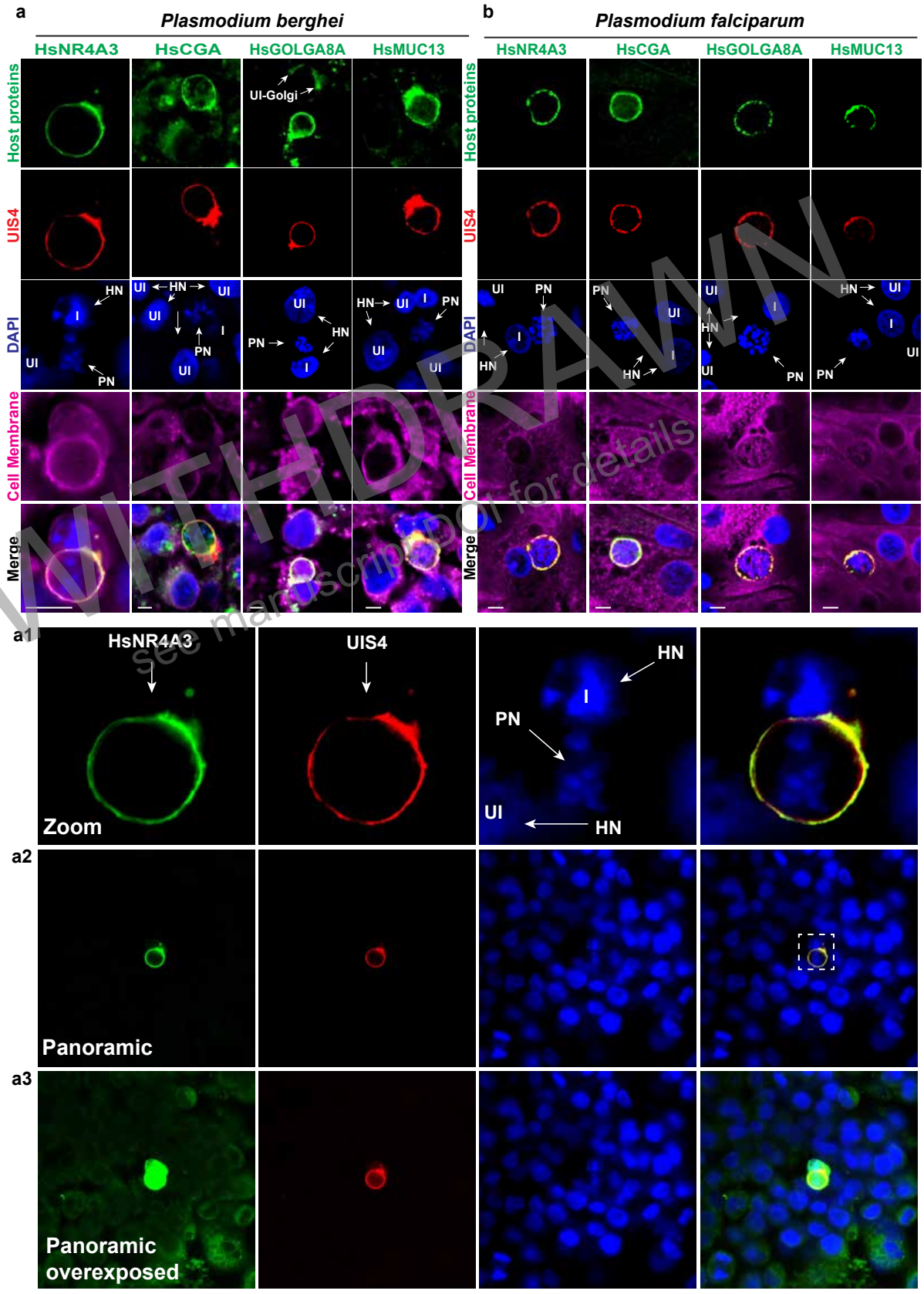

41

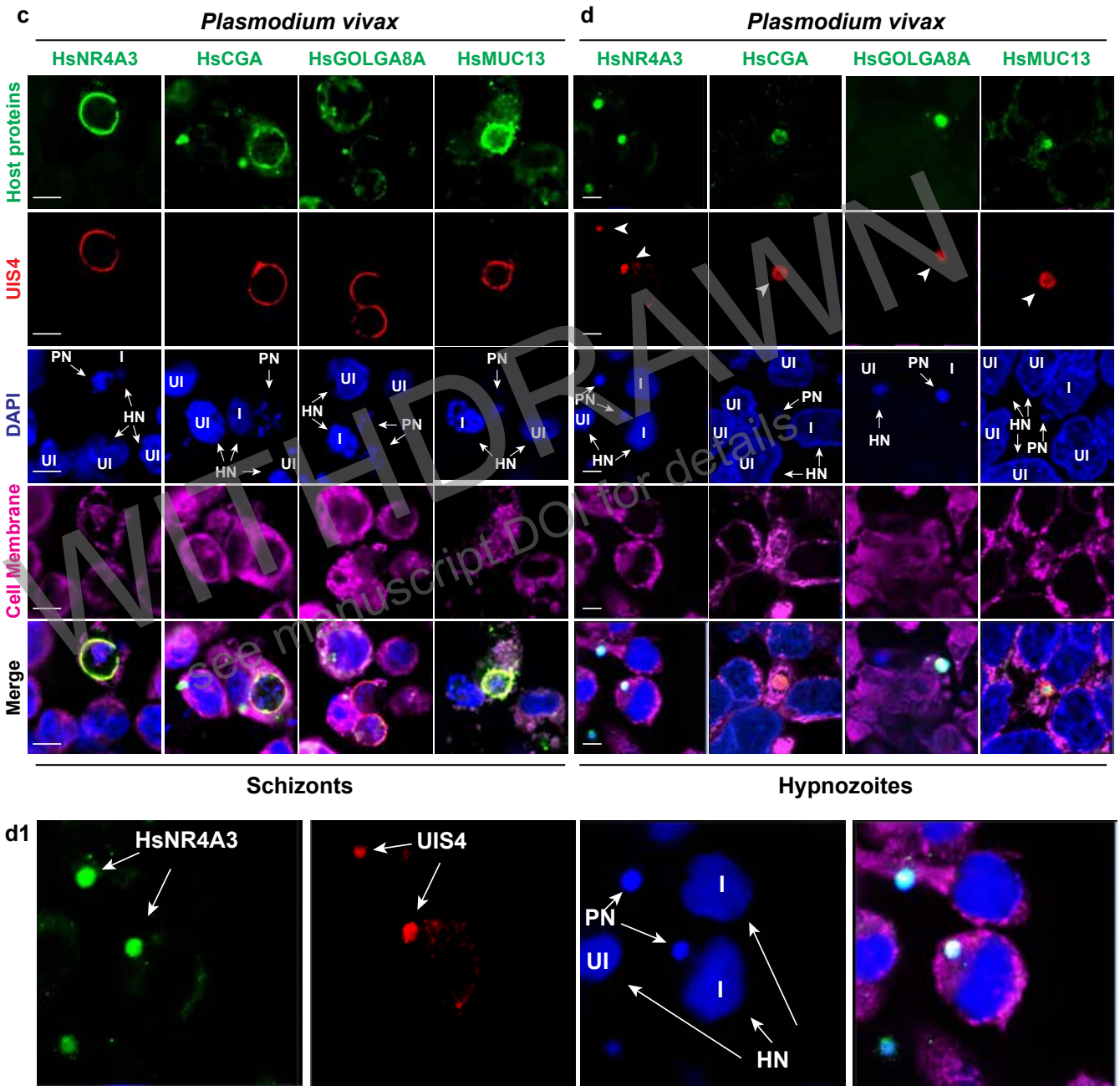

Figure 2

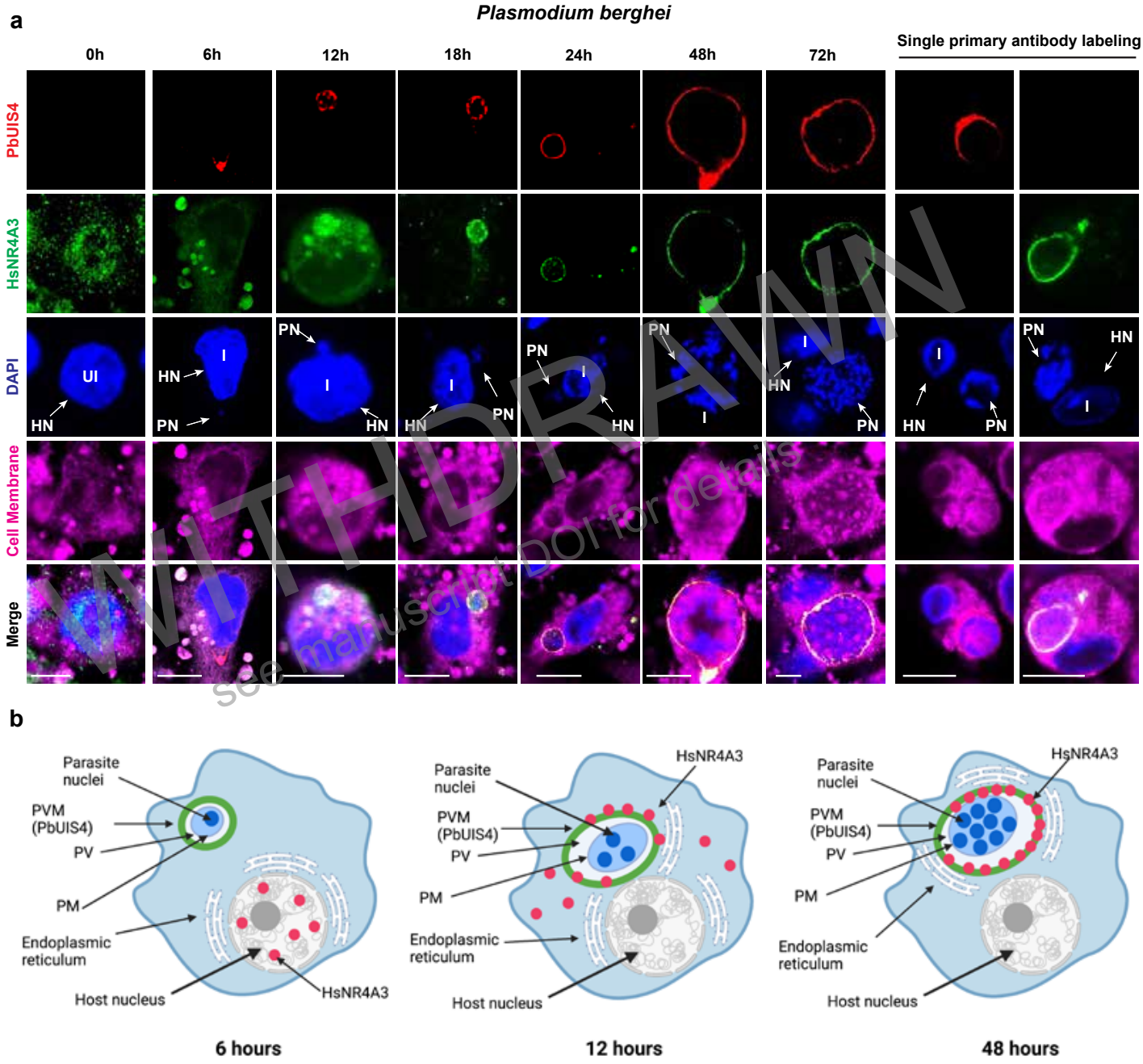

Figure 3

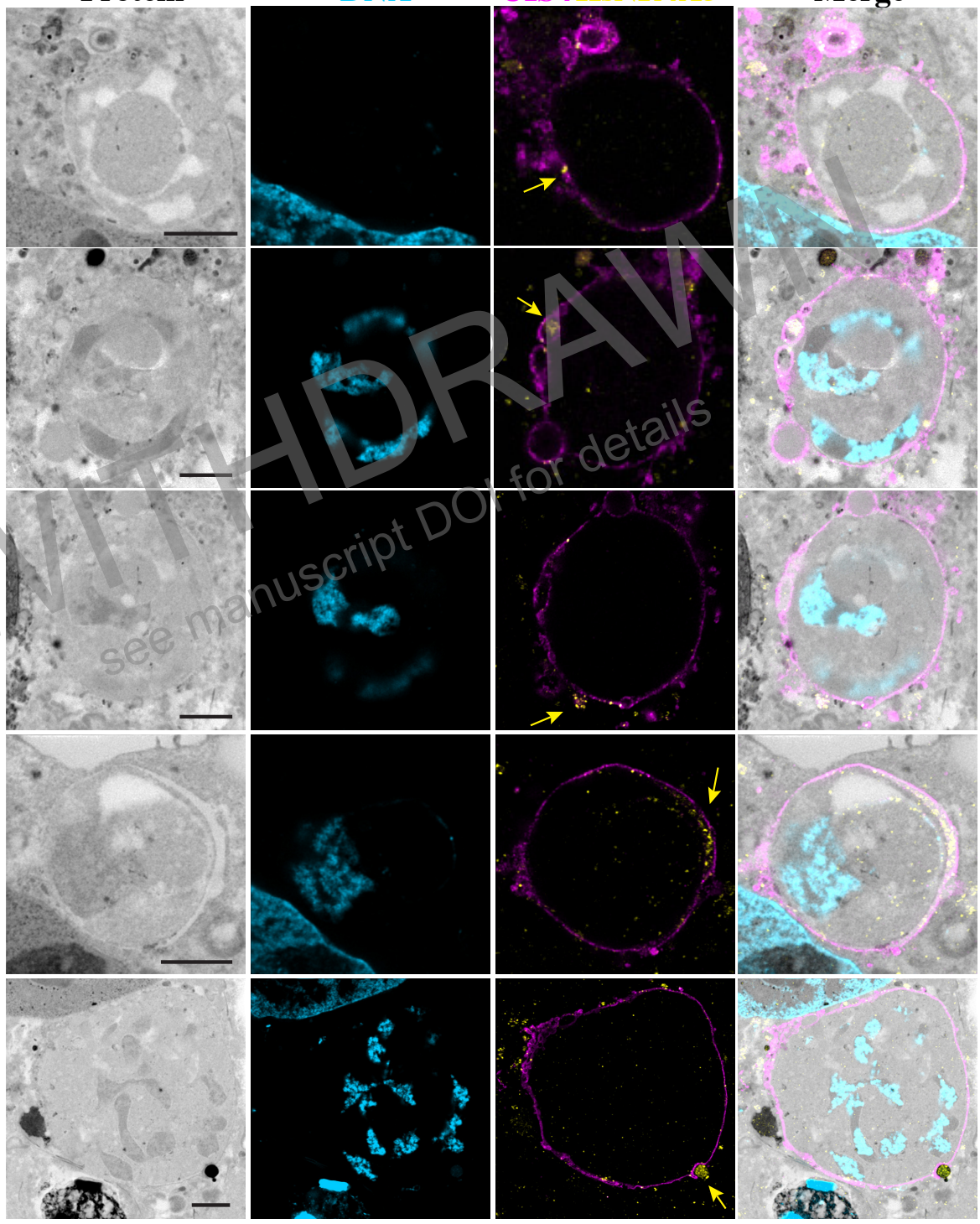

Figure 4

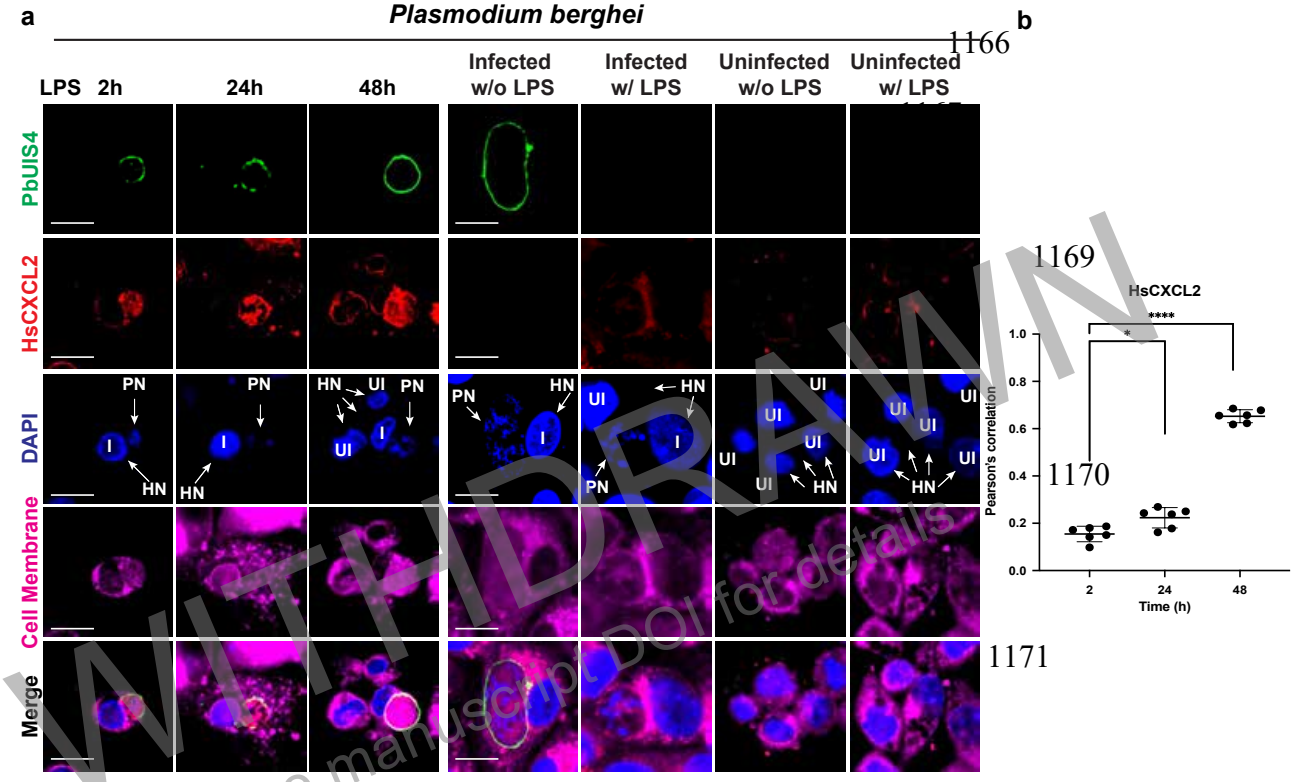

Figure 5